



# Improving historical trends in the INFERNO fire model using the Human Development Index

João C. M. Teixeira<sup>1,2,4</sup>, Chantelle Burton<sup>1</sup>, Douglas I. Kelley<sup>3</sup>, Gerd A. Folberth<sup>1</sup>, Fiona M. O'Connor<sup>1,2</sup>, Richard A. Betts<sup>1,2</sup>, and Apostolos Voulgarakis<sup>4,5</sup>

<sup>1</sup>Met Office, Fitzroy Road, EX1 3PB, Exeter, UK

<sup>2</sup>Global Systems Institute, Department of Mathematics & Statistics, University of Exeter, EX4 4QE, UK

<sup>3</sup>UK Centre for Ecology and Hydrology, Wallingford OX10 8BB, U.K

<sup>4</sup>Leverhulme Centre for Wildfires, Environment and Society, Department of Physics, Imperial College London, London, UK

<sup>5</sup>School of Environmental Engineering, Technical University of Crete, Chania, Greece

**Correspondence:** João C. M. Teixeira ([joao.teixeira@metoffice.gov.uk](mailto:joao.teixeira@metoffice.gov.uk))

**Abstract.** Earth System Models (ESM), have struggled to reproduce the historical decline in burnt area, with discrepancies largely attributed to the under-representation of anthropogenic fire suppression. Key factors such as agricultural expansion, land-use changes, fire management policies, and landscape fragmentation have all contributed to reduced fire activity, especially in tropical savannas, but these are not adequately captured in the fire model formulation that underpins most ESMs. This study  
5 investigates whether the observed downward trend in global burnt area can be better represented in the JULES-INFERNO fire model by incorporating a simplified representation of direct human impacts on fire. Specifically, we focus on the Human Development Index (HDI), which reflects socio-economic development and, in turn, influences fire suppression efforts. By incorporating HDI into INFERNO, we aim to improve the representation of fire ignition and suppression dynamics. Results show that including HDI-driven socio-economic factors reduces biases in annual burnt area, particularly in Temperate North  
10 America, Central America, and Europe. While including HDI corrects regional biases, it also introduces a global negative bias as compensating errors at the regional level are addressed. Overall, this approach improves the representation of burnt area trends in eight out of 14 regions, including Southern Hemisphere South America and Northern Hemisphere Africa, where observations show negative trends. Despite mixed results in other fire regions, this study demonstrates that incorporating a socio-economic dimension in INFERNO through HDI provides a simple and effective way to improve fire model performance.  
15 It also enhances the ability of ESMs to capture human-environment interactions and offering valuable insights for future climate modelling and fire management strategies.

## 1 Introduction

Globally, burnt area trends are influenced by complex interactions between climate change, human activities, and natural ecosystem processes, resulting in large variability over the past few decades. However, the long-term trend (e.g., 1997 - 2016)  
20 has shown an overall decline in global burnt area, especially driven by changes in burnt area of African savannas and grasslands (decline of 1.27 % per year). The trend, shown in Figure 1 b), is attributed to changes in land use, particularly agricultural



expansion and intensification in savanna and grassland regions, which reduces the availability of fuel for fires (Riley et al., 2019; Andela et al., 2017).

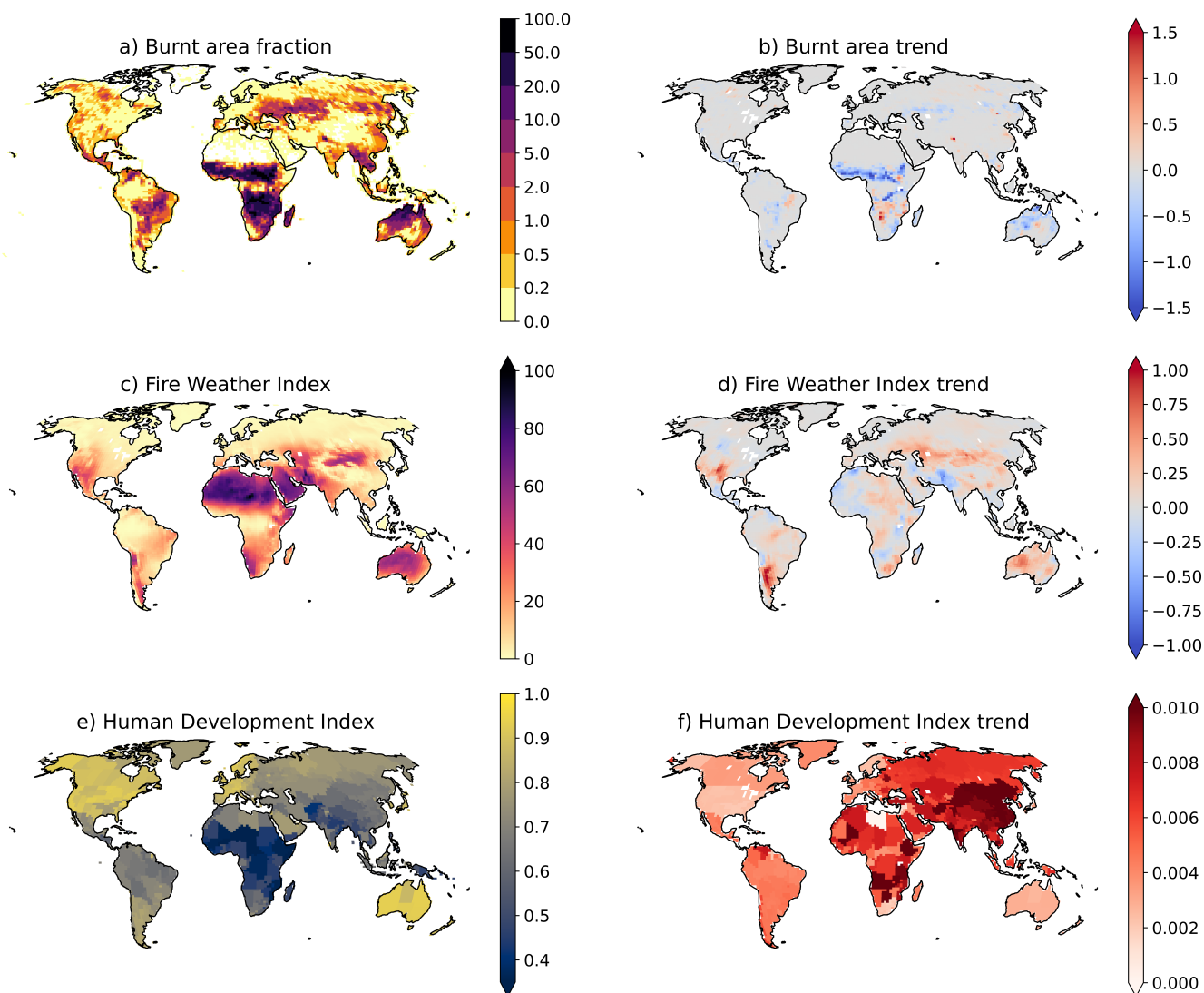


**Figure 1.** Global distribution of a) Burnt area fraction - GFED4s - (%) total annual average (1997 - 2016) and b) respective trend ( $\% \text{ year}^{-1}$ ); c) Fire Weather Index average (1997 - 2016) and d) respective trend ( $\text{year}^{-1}$ ); e) Human Development Index average (1997 - 2016) and f) respective trend ( $\text{year}^{-1}$ ).

Climate is a key factor that also influences fire activity (Archibald et al., 2010; Andela et al., 2017; Jones et al., 2022; Kelley et al., 2019). Rising temperatures are leading to longer fire seasons, particularly in temperate and boreal regions (Sullivan et al., 2022; Jones et al., 2024). Additionally, reduced rainfall during the critical phase of fire seasons increases the likelihood of large-scale fires, while increased rainfall during certain times of the year can promote vegetation growth, providing more



fuel for future fires. However, while climate strongly influences inter-annual variability and is increasingly important for long-term trends, particularly in temperate and boreal regions, human activity—such as land use change, agricultural expansion, and active fire suppression—has been the dominant driver of long-term declines in global burnt area, especially in tropical savannas (Riley et al., 2019; Andela et al., 2017).

Furthermore, human population density and prosperity can significantly impact burnt areas. (Andela et al., 2017) show that due to population growth, socioeconomic development, and the increased demand for agricultural products in regional and global markets, there has been a shift towards more capital-intensive agriculture, resulting in fewer and smaller fires. These factors have a predictable impact on the use of fire, with a strong inverse correlation between the area burned and economic development.

The study by Li et al. (2024) shows that the Earth System Models (ESMs) used to provide state-of-the-art climate projections for Phase 6 of the Coupled Model intercomparison Project (CMIP6; Eyring et al. (2016)) fail to reproduce the decline in global burned area and fire carbon emissions observed over the past two decades. They identify the primary reason for this discrepancy as an underestimation of anthropogenic fire suppression in fire models. Key human-driven factors - such as agricultural expansion, land-use changes, fire management policies, and landscape fragmentation - have significantly reduced fire activity, particularly in tropical savannas (Andela et al., 2017). However, most CMIP6 models do not adequately account for these suppression mechanisms, resulting in an overestimation of burned area and fire-related carbon emissions.

Most global fire models, such as JULES-INFERNO (Mangeon et al., 2016; Burton et al., 2019), apply simplistic representations of human ignitions, generally specified as a function of population density, increasing up to a threshold value after which there are no additional ignitions with an increasing population (Rabin et al., 2017; Teckentrup et al., 2019; Ford et al., 2021). This approach does not account for the impacts of socio-economic factors on anthropogenic fire ignitions or suppression. It also does not capture how humans influence regional variation in contemporary burning practices.

This misrepresentation has important implications for climate projections and carbon cycle modelling, and emphasizes the need for better integration of dynamic human influences on fire regimes, such as incorporating evolving socio-economic factors (e.g., population growth, infrastructure expansion, and fire suppression strategies) into fire models (Li et al., 2024).

The Human Development Index (HDI) is a composite measure that combines four key metrics: life expectancy at birth, expected years of schooling, average years of schooling, and Gross National Income (GNI) per capita (Bhanojirao, 1991). These metrics are normalized by their respective maximum values, and the HDI is calculated as the geometric mean of life expectancy, education, and GNI per capita. The HDI has been used in various studies to better understand the socio-economic impacts on the Earth System (ES) (Türe, 2013; Hickel, 2020; Roy et al., 2023).

HDI is strongly correlated with inter-annual variability in burned area. Chuvieco et al. (2021) shows that higher HDI is associated with lower fire activity, driven by reduced dependence on fire for agricultural purposes due to increased mechanization and a shift away from agrarian livelihoods. In contrast, regions with lower HDI exhibit more consistent fire activity, reflecting continued reliance on fire as a land management tool. The study also demonstrated that incorporating socio-economic indicators like HDI into fire models significantly improves their ability to reproduce observed patterns of fire variability.



Additionally, Li et al. (2013) and Zou et al. (2019) investigated the use of Gross Domestic Product (GDP) to parametrise human influences on fires. However, their approach was limited to agricultural fires and did not account for broader human factors in fire management.

65 Human influences on fire activity have become more pronounced since the late 18<sup>th</sup> century, reflecting the effects of industrialization, climate change, land clearance, population growth, the replacement of traditional fire management practices, and the development of large-scale firefighting and fuel management in the 20<sup>th</sup> century (Bowman et al., 2020). This demonstrated the need for improved data collection to better quantify and model fire activity and human populations, including their socio-economic status and historical, cultural, and political legacies. As vegetation fires' economic and environmental impacts  
70 are likely to worsen due to anthropogenic climate change (Sullivan et al., 2022; Jones et al., 2024; Haas et al., 2024), this is increasingly urgent. Additionally, Nikolakis and Roberts (2022) examined how policy learning occurs in wildfire governance, focusing on how wildfire policies in British Columbia have evolved. Their case study shows that policy transfer from similar contexts, particularly Indigenous peoples and their governments, can reshape perceptions of wildfire risk and solutions as we adapt to an uncertain future. Similarly, Pandey et al. (2023) explored the complexity of socio-economic factors on fire and  
75 the varied fire management policies worldwide, demonstrating that despite differences, these policies have led to a gradual reduction in fire occurrences and burned area over time.

Several studies have shown that in developed regions, land and fire management policies play a more significant role in controlling fire ignitions than other human behaviours (Nikolakis and Roberts, 2022; Jacobson et al., 2022; Ford et al., 2021; Curt and Frejaville, 2018; Carreiras et al., 2014; Mourão and Martinho, 2014). Notably, Curt and Frejaville (2018) found that  
80 wildfire policies in Mediterranean France have led to a nearly linear decrease in the number of fires since 1975, though the burnt area has fluctuated more abruptly. Therefore, representing land and fire management policies in global fire models is crucial to building confidence in the modelling frameworks which are used to understand future climate regimes. This, in turn, can underpin decision-making by policy-makers in regards to fire policy in the future.

Nonetheless, how socio-economic factors impact on fires is complex and dependent on many factors that are difficult to  
85 represent in an ESM context. These factors depend on policies implemented at government level, as well as cultural behaviour which varies widely across the world. As a result, the formulation of Climate and ES models does not allow for representing these details.

Rather than attempting to capture the full complexity of socio-economic influences on fire, this study explores a simplified, emergent relationship—using HDI as a proxy—that is better suited for large-scale applications. We use observed datasets of  
90 HDI, burnt area, and fire weather index to derive a relationship between HDI and burnt area, and model data to devise an approach to implement these in the INFERNO fire model. A detailed description of the observed datasets is provided in the Appendix, section A1.

In Section 2, we explore the relation between HDI and burnt area and describe the INFERNO fire model, the coupling of INFERNO to the latest representation of the land surface model (JULES-ES) as used in the UK's Earth System Model  
95 (UKESM1), and how we include HDI into INFERNO's ignition scheme. In Section 3, we evaluate the impact of considering HDI on burnt area, burnt area trends, as well as the impact of external model drivers of burnt area trends. Discussion and



conclusions from this work are presented in Section 4 where we focus on novel model results, placing the link between socio-economic factors and fires in context with existing literature. Model limitations and known issues are also highlighted.

## 2 Methods

### 100 2.1 Relation between HDI and Burnt Area

As climate is a dominant factor influencing fire activity, it is essential to first account for and remove climate change's influence before exploring the effects of socio-economic factors on burnt area. For this, and considering that the Fire Weather Index (FWI) depends solely on the weather variables that drive fire activity, we apply a linear regression model to the FWI data, and the predicted slope from this linear regression model is then removed from the normalised values of burnt area. A normalised  
105 burnt area dataset is produced with the influence of climate removed (deweathered), and used to analyse how socio-economic factors, through the use of HDI, impact fire activity.

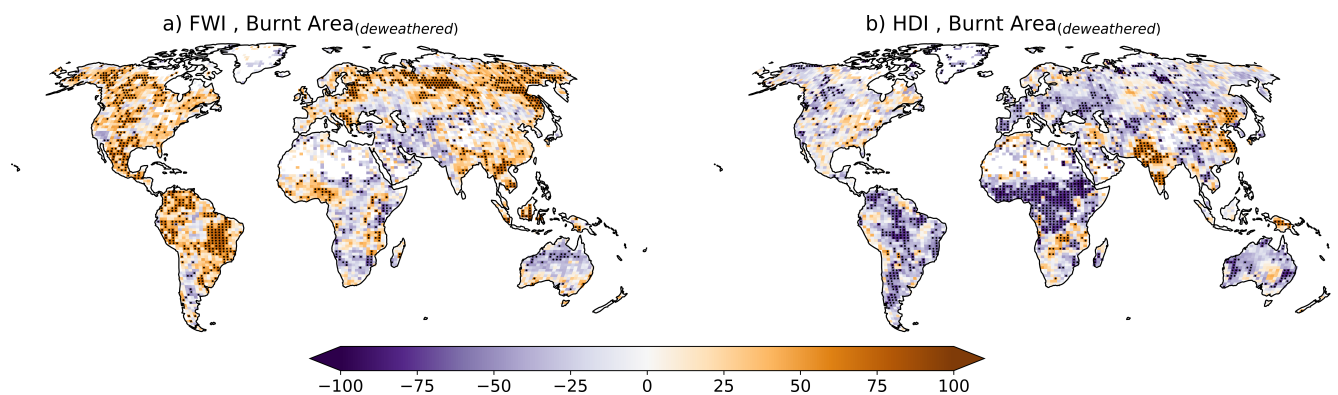


**Figure 2.** Pearson correlation (%) between the monthly mean (1997 - 2016) a) FWI and the deweathered Burnt Area (GFED4s), and b) HDI and the deweathered Burnt Area (GFED4s). Stippling is shown for points where the Pearson correlation is statistically significant with a 95 % confidence level.

Figure 2 shows the spatial correlation coefficient between FWI and deweathered burnt area (panel a) and between HDI and deweathered burnt area (panel b). Although the spatial correlation coefficient between FWI, HDI, and the deweathered burnt area are spatially varied - Figure 2 - there is a stronger negative correlation between HDI and the deweathered burnt area for most of the globe, relative to what is found for FWI, except for the Indian subcontinent and Eastern China, which shows a  
110 positive correlation. The relation between HDI and the deweathered burnt area is especially evident over Eurasia, continental North America, central Asia, Southern Africa, and Australia. For these regions, despite the increases in FWI, burnt area has shown a variety of negative regional trends highly correlated with HDI (Figure 1 and 2). Nonetheless, the deweathered burnt area shows a strong positive correlation over the boreal regions of North America and Siberia, as well as the Cerrado ecoregion  
115 of South America.

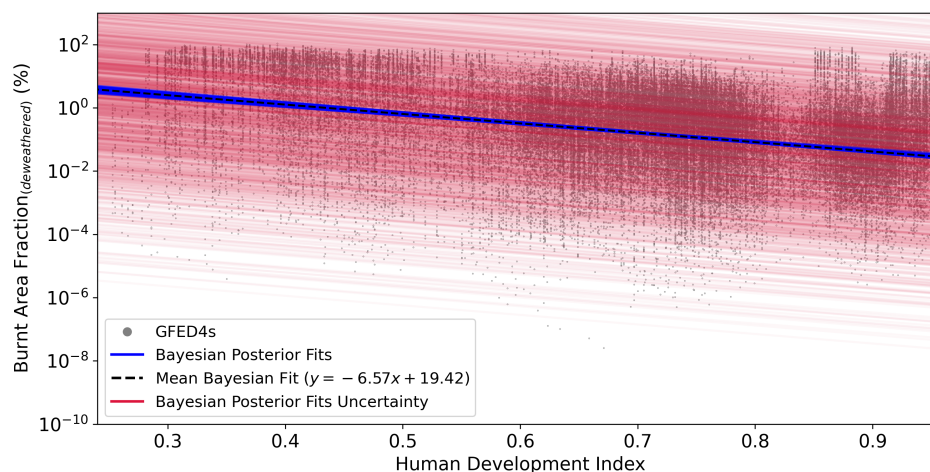


**Figure 3.** Relation between the between the monthly mean (1997 - 2016) HDI and the log transform burnt area fraction (%) for GFED4s. The grey dots represent the GFED4s burnt area fraction in function of HDI, the Bayesian regression posterior fits is represented in blue solid lines, the mean Bayesian fit is represented in the black dashed line, and the uncertainty from the Bayesian posterior fits residuals is represented in the red solid lines.

Multiple techniques are used to further investigate the relationship between HDI and burnt area. The scatter plot of the deweathered burnt area against HDI in log-transformed space is presented in Figure 3. Due to the inherent stochasticity of burnt area, the results show a wide range of values, spanning small to large relative burnt area fractions for any given HDI. To account for this variability, and isolate the effects of HDI on burnt area, we applied a Bayesian Linear Regression method (Klauenberg et al., 2015) to the log-transformed burnt area fraction, denoted by  $\log(BA^*)$ :

$$\log(BA^*) \sim BA_0 + \delta BA \times HDI \quad (1)$$

where  $BA_0$  is the burnt area intersect at  $HDI = 0$  and  $\delta BA$  is the change, or slope, in burnt area with HDI. We optimise using a No U-Turn Sampler (NUTS) optimisation over a normal posterior distribution, using the PyMC Python package, as per Kelley et al. (2019).

The priors for our two regression parameters were largely uniformed, with  $BA_0$  having a normal distribution, with a mean of zero and a standard deviation of 25, and  $\delta BA$  having a log-normal distribution with mean of zero and standard deviation of ten.

We utilise 1000 Bayesian posterior model fits (with 145 samples represented by the solid blue line in Figure 3), effectively capturing the uncertainty in the data while estimating the association between HDI and burnt area.

This method show that the observations show a linear decline in burnt area with increasing HDI, with a mean slope of -6.57 (%).



## 2.2 INFERNO fire model

In this work we simulate fire using the INFERNO (INteractive Fires and Emissions algoRithm for Natural envirOnments; Mangeon et al. (2016)) fire model. INFERNO uses an approach based on Pechony and Shindell (2009), adapted to allow interactions within an ESM framework. More precisely, INFERNO uses water vapour pressure deficit as one of the main indicators of flammability and an inverse exponential relationship to relate flammability to soil moisture.

$$BA_{PFT} = I_T F_{PFT} \overline{BA_{PFT}} \quad (2)$$

where  $I_T$  represents the fire ignitions, including natural and human ignitions as well as fire suppression by humans,  $F_{PFT}$  the flammability per PFT dependent on the 1.5 m temperature, 1.5 m relative humidity and fuel density - as defined in Eq. 4 through 6 from Mangeon et al. (2016) - and  $\overline{BA_{PFT}}$  is the average burnt area for each PFT.

The burnt area, represented in Eq. 2, is associated with an average burnt area per fire for each model plant functional type (PFT). This decouples the fire spread stage from local meteorology and topography, processes not typically resolved in coarse grids, such as those often used within ESMs.

It should be noted that the recent work by Haas et al. (2022) shows that topography and wind speed have an impact on fire size even when aggregated to a 0.50° grid cell scale. However, the resolution of the model used in this study is significantly coarser approximately 1.75°.

INFERNO fire ignitions are split into Natural Ignitions ( $I_N$ ) from cloud to ground lightning flashes and from Human activities ( $I_A$ ) dependent on population density ( $PD$ ) as described in Eq. 3. Humans are also responsible for suppressing fires in the model, using a suppression function ( $f_{NS}$ ) dependent on human population density (Eq. 4) to represent the fraction of fires not suppressed by humans. The total ignitions ( $I_T$ ) are represented by Eq. 5.

$$I_A = k_{(PD)} PD \alpha \times (\mathbf{1} - \mathbf{HDI}) \quad (3)$$

$$f_{NS} = 7.7 (c_1 + c_2 \times e^{-\omega PD}) \times (\mathbf{1} - \mathbf{HDI}) \quad (4)$$

$$I_T = (I_N + I_A) \frac{f_{NS}}{8.64 \times 10^{10}} \quad (5)$$

where  $k_{(PD)} = 6.8 \times PD - 0.6$  is a function that represents the varying anthropogenic influence on ignitions in rural versus urban environments, and the parameter  $\alpha = 0.03$  represents the number of potential ignition sources per person per month per  $km^2$ , and  $HDI$  represents the Human Development Index.

In Equation 4 the fraction of fires that remain unsuppressed at the most populated areas is expressed by  $c_1$ . The maximum number of fires that remain unsuppressed at the distant, unpopulated regions is defined by the sum of  $c_1$  and  $c_2$ , and the rate



at which the number of unsuppressed fires decreases with increasing population density is determined by  $\omega$ . As expressed  
160 by Pechony and Shindell (2009), due to the lack of global quantitative data, constant values are selected in a rather heuristic  
manner:  $c_1 = 0.05$ ,  $c_2 = 0.9$ , and  $\omega = 0.05$ . In this way, up to 95 % of fires are assumed to be suppressed in densely populated  
regions, and 95 % are assumed to remain unsuppressed in unpopulated regions.

Previously, INFERNO only included information on population density. To represent the socio-economic factors impacting  
fire ignition and suppression, we include a HDI term ( $1 - HDI$ ) in our human ignition and suppression Eq. 3 and 4 (shown  
165 in bold). In addition it should be noted that the HDI implementation scales both  $c_1$  and  $c_2$  according to the HDI value of any  
given grid point.

This approach does not directly implement the empirical relationship established from observational data in Section 2.1.  
Instead, it introduces an HDI dependent formulation based on the assumption that ignition rates decrease and suppression  
increases with higher HDI. This reflects the hypothesis that more developed regions experience fewer ignitions and greater fire  
170 control capacity. We then test whether this indirect implementation can reproduce the observed relationship between burned  
area and HDI.

Despite being a simple representation, it aligns with the few studies found in literature that looked at the impact governmental  
policies have on prevention of wildfires (e.g., the work by Curt and Frejaville (2018)). Furthermore, although the equations  
used could be adjusted to provide the best results, we avoid this approach in this first implementation in INFERNO to avoid  
175 masking compensating biases that are existent or could arise from this implementation.

In this representation of socio-economic impacts on fire ignition and suppression, we assume that fire ignitions decrease and  
fire suppression increases for areas with more effort in human development improvements. Moreover, it reduces the impact  
changes in population density have in areas with high HDI while keeping a dependency on population density changes for areas  
with low HDI, where policies on land and fire management have a greater role than other human behaviours in controlling  
180 ignitions (Nikolakis and Roberts, 2022; Ford et al., 2021; Jacobson et al., 2022; Carreiras et al., 2014; Mourão and Martinho,  
2014). The impact of HDI on INFERNO anthropogenic fire ignitions, represented as  $I_A$  (Eq. 3), is depicted in Figure 4.

We obtained HDI data from the gridded global datasets for Gross Domestic Product and Human Development Index (Kummu  
et al., 2018), which provides HDI data from 1990 to 2015. To cover the full modelled period (1860-2016), the HDI data is  
linearly ramped from the minimum HDI value of the dataset (0.2) to its value in 1990 for each grid point. The original HDI  
185 dataset was spatially interpolated using a nearest-neighbor interpolation method to match the model grid, and was updated at  
the same frequency as the original dataset - annually.

### 2.3 JULES-ES and INFERNO

We use the community land surface model JULES (Joint UK Land Environment Simulator; Clark et al. (2011); Best et al.  
(2011)) at version 5.7, with the science configuration of the land surface as used in UKESM1 (Sellar et al., 2019a), includ-  
190 ing 13 PFTs, and dynamic vegetation from TRIFFID (Top-down Representation of Interactive Foliage and Flora Including  
Dynamics; Cox et al. (2000); Cox (2001)). This ES configuration of JULES is known as JULES-ES (Mathison et al., 2022).  
JULES simulates surface fluxes of water, energy, as well as vegetation and carbon. Here, we use JULES as a stand-alone offline

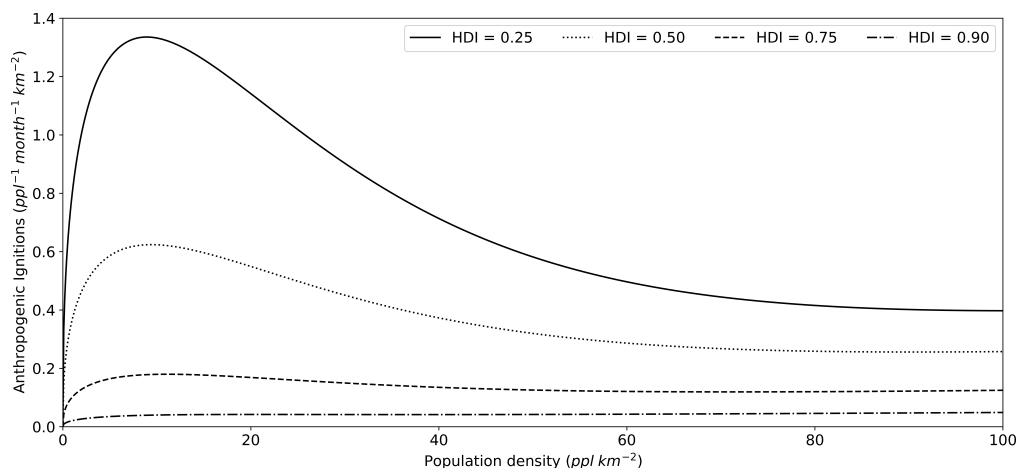


**Figure 4.** Anthropogenic fire ignitions ( $ppl^{-1} month^{-1} km^{-2}$ ) as a function of population density ( $ppl km^{-2}$ ) and Human Development Index.

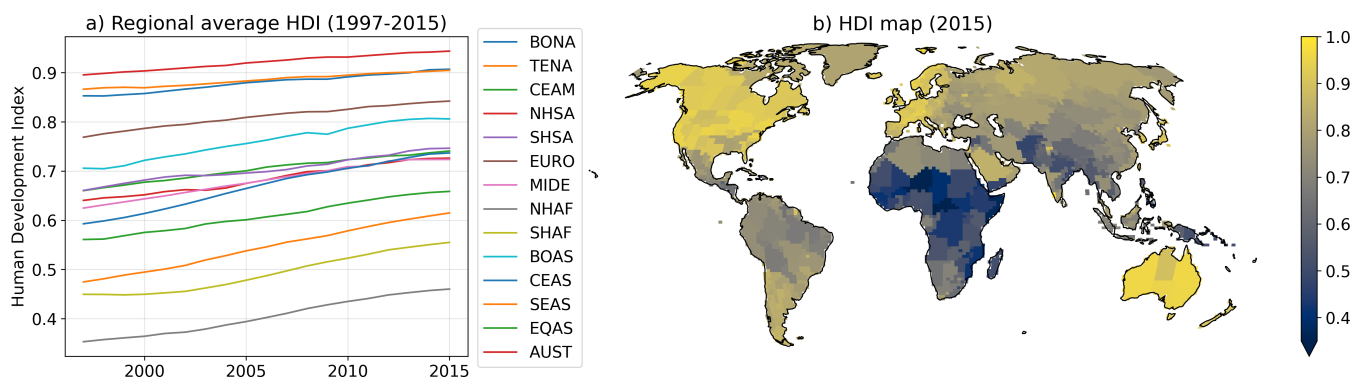


**Figure 5.** RegridDED HDI as provided to JULES-INFEERNO+HDI. a) regional average for the 1997-2015 period and b) spatial distribution for the year 2015. The regions depicted in a) are described in Figure A1.

model run at a spatial resolution of N96 (equivalent to a horizontal resolution of 135 km in the mid-latitudes). The Climate Research Unit - National Centers for Environmental Predictions reanalysis (CRU-NCEP v7) (Harris et al., 2014; Viovy, 2018) atmospheric variables are provided at 6-hourly intervals to drive JULES, including carbon dioxide ( $CO_2$ ), precipitation, temperature, specific humidity, wind, air pressure, and short and long wave radiation. The model runs from 1860–2016 with this forcing. In this work, we analyse the period that overlaps with observations (1997-2015).

We use the latest fire-vegetation coupling described in Burton et al. (2019) and Burton et al. (2020), incorporating additional feedbacks to the carbon cycle from litter and vegetation burning. This setup includes mortality due to fire by plant functional type (PFT), which is set to 40 % for trees, 60 % for shrubs, and 100 % for grasses. This setup differs from that used in Teixeira et al. (2021), where no fire-vegetation feedbacks were considered.



205 Fire ignitions are based on population density data from HYDE 3.2 (Klein Goldewijk et al., 2017); (Goldewijk et al., 2017) and monthly lightning flashes climatology from LIS-OTD (Lightning Imaging Sensor – Optical Transient Detector; Cecil (2006)) observations over 1995-2014, regrided from 0.5° resolution to N96 (1.25° 1.25 latitude × 1.875° longitude). After spinning up the model to equilibrium, we complete a full historical simulation from 1860-2019 at N96 and use results from the present day (1997-2015) for our analysis to compare with available observations of burnt area.

We performed two model experiments to test the impact of representing the socio-economic factors on fire ignition and suppression in INFERNO. A control experiment referred to as JULES-INFERNO, and a similar experiment, including socio-economic factors on fire ignition and suppression parametrisation described in section 2.2, referred as to JULES-INFERNO+HDI.

210 Socio-economic impacts on fire are not represented in the initial formulation of INFERNO described in Mangeon et al. (2016) for the ignitions and suppression of fires. This is reflected in the  $\overline{BA_{PFT}}$  values used in the initial implementation of INFERNO. Posterior work by Andela et al. (2019) shows that average burnt area values can be larger than the ones used in the work of Mangeon et al. (2016).

**Table 1.** Biomass burning average burnt areas ( $km^2 fire^{-1}$ ) for various plant functional types based on Burton et al. (2019) (top row) and adapted from Andela et al. (2019) (bottom row).

	Broadleaf tree			Needleleaf tree		C3			C4			Shrubs	
	Deciduous	Evergreen		Evergreen	Deciduous	Grass	Crop	Pasture	Grass	Crop	Pasture	Deciduous	Evergreen
$\overline{BA_{PFT}}$	1.7	Tropical	Temperate	1.7	1.7	3.2	0.4	3.2	3.2	0.4	3.2	2.7	2.7
Revised $\overline{BA_{PFT}}$	5.2	1.4	2.5	5.2	5.2	10.2	1.4	1.4	10.2	1.4	1.4	5.1	5.1

215 When the HDI-based parametrisation of socio-economic impacts on fire is included in INFERNO, it reduces ignitions and suppression of fires. Therefore, the values of  $\overline{BA_{PFT}}$  are adapted to align with those reported by Andela et al. (2019). This was achieved by deriving the PFT-specific values by matching those reported by Andela et al. (2019) to the PFT categories represented in JULES as much as possible. These are not direct comparisons and a balance between the PFT representation of the region in JULES was used to estimate a reasonable average burnt area for INFERNO. The  $\overline{BA_{PFT}}$  values in both experiments are detailed in Table 1.

## 220 2.4 Burnt area evaluation

To analyse the model performance, we calculated the following statistical and error measures, relative to the observed (GFED4s) and modelled (JULES-INFERNO and JULES-INFERNO+HDI) burnt area:

- Deviation of the modelled data in relation to observed values:

$$\phi'_i = \phi_i - \phi_{i,obs} \quad (6)$$

- 225 – Bias, which represents the mean deviation of the modelled data in relation to the observed values.

$$Bias = \frac{1}{N} \sum_{i=1}^N \phi'_i \quad (7)$$



- The Root Mean Square Error.

$$RMSE = \sqrt{\frac{\sum_{i=1}^N (\phi_i - \phi_{i,obs})^2}{N}} \quad (8)$$

- The Root Mean Square Error after the removal of a constant bias.

230

$$RMSE_{UB} = \sqrt{\frac{\sum_{i=1}^n [(\phi_i - \bar{\phi}) - (\phi_{i,obs} - \bar{\phi}_{obs})]^2}{N}} \quad (9)$$

- Standard deviation for the modelled - equation 10 - and observed - equation 11 - data.

$$STD = \sqrt{\frac{\sum_{i=1}^n (\phi_i - \bar{\phi})^2}{N}} \quad (10)$$

$$STD_{obs} = \sqrt{\frac{\sum_{i=1}^n (\phi_{i,obs} - \bar{\phi}_{obs})^2}{N}} \quad (11)$$

were  $i$  is the temporal index and  $N$  is the number of elements of  $\phi$  considered, and  $\bar{\phi}$  is the constant bias.

235 Considering these statistics, a perfect simulation would have the following criteria:

- RMSE = 0
- RMSE<sub>UB</sub> = 0
- bias = 0
- Pearson correlation = 100 %
- 240 - STD / STD<sub>GFED4s</sub> = 1
- RMSE / STD<sub>GFED4s</sub> = 0
- RMSE<sub>UB</sub> / STD<sub>GFED4s</sub> = 0

### 3 Results

#### 3.1 Representing Burnt Area - HDI relationship in INFERNO

245 The posterior fit distributions of the Bayesian Linear Regression parameters slope, intercept and sigma (additional noise caused by none HDI drivers) in Figure 3 and A2 show narrow intervals for the posterior parameters, evidence of high confidence in



the fit for a linear relationship between HDI and deweathered burnt area fraction, with the mean Bayesian fit (dashed black line) presenting a slope of  $-6.57 (\%^{-1})$ , and an intercept of  $19.42 (\%)$ .

In summary, this analysis reveals a strong relationship between the HDI and burnt area (Figure A2). It demonstrates a predominantly negative correlation between HDI and deweathered burnt area globally, and especially in Eurasia, continental North America, central Asia, Southern Africa, and Australia, where increases in FWI have not translated into higher burnt areas (Figure 2). Conversely, positive correlations persist in regions like the boreal areas of North America, Siberia, and the Cerrado of South America. This evidence highlights that HDI can be used as an indicator of the role socio-economic factors play in mitigating fire activity.

To evaluate the use of HDI as a proxy for representing socio-economic factors influencing fire ignition and suppression in INFERNO, the methodology described in Section 2.1 was applied, and the results are presented in Figure 6, and the distribution of its posterior fits can be found in Figure A2.

As expected, JULES-INFERNO (the original version of the model not including the HDI) does not present a strong relationship between the deweathered burnt area fraction and HDI. The mean Bayesian fit slope is  $-2.75 (\%)$ , indicating a weaker relationship between the variables than in JULES-INFERNO+HDI when compared to observations. In contrast, the stronger negative slope of  $-6.57 (\%^{-1})$  found in observations suggests a more pronounced socio-economic influence on fire suppression in the observational data. When HDI is explicitly incorporated to represent socio-economic effects on fire in JULES-INFERNO+HDI, the model better reproduces the relationship observed in GFED4s, with a Bayesian fit slope of  $-5.40 (\%^{-1})$ . This result demonstrates an improved representation of the socio-economic impact on fire dynamics, aligning the model more closely with observations.

### 3.2 Evaluation of impact on burnt area

To better understand the regional impact of implementing the socio-economic factors on fire ignition and suppression in INFERNO, we focus on the burnt area results averaged over the GFED4s regions as defined in Figure A1.

Both model experiments reproduce the overall geographical pattern of the annual average burnt area fraction (Figure 7), though with some regional differences compared to observations. For instance, JULES-INFERNO simulates the observed pattern in the major fire regions: South America, Africa and Eurasia. The 2-D cross-correlation was used to determine what is referred to as spatial correlation between the model experiments and the observation data. JULES-INFERNO shows substantial spatial biases over North America, Europe and Asia, leading to a low global spatial correlation of  $26.5 \%$  compared with GFED4s. Conversely, JULES-INFERNO+HDI reduces fires in the regions with higher HDI values, reducing the biases seen in JULES-INFERNO and resulting in a better agreement with GFED4s. JULES-INFERNO+HDI has a global spatial correlation of  $46.5 \%$  when compared with GFED4s. However, due to the nature of the HDI data, sharp boundaries between countries can appear in the burnt area results (e.g., between Canada and the United States of America) - 1 e).

Including socio-economic factors in the parametrisation for fire ignition and suppression has an impact in all regions. However, it mostly reduces the burnt area in regions with high prosperity (high values of HDI), leading to improvements over North America, Europe and Asia, as shown in Figure 8. Moreover, compared to JULES-INFERNO, JULES-INFERNO+HDI reduces

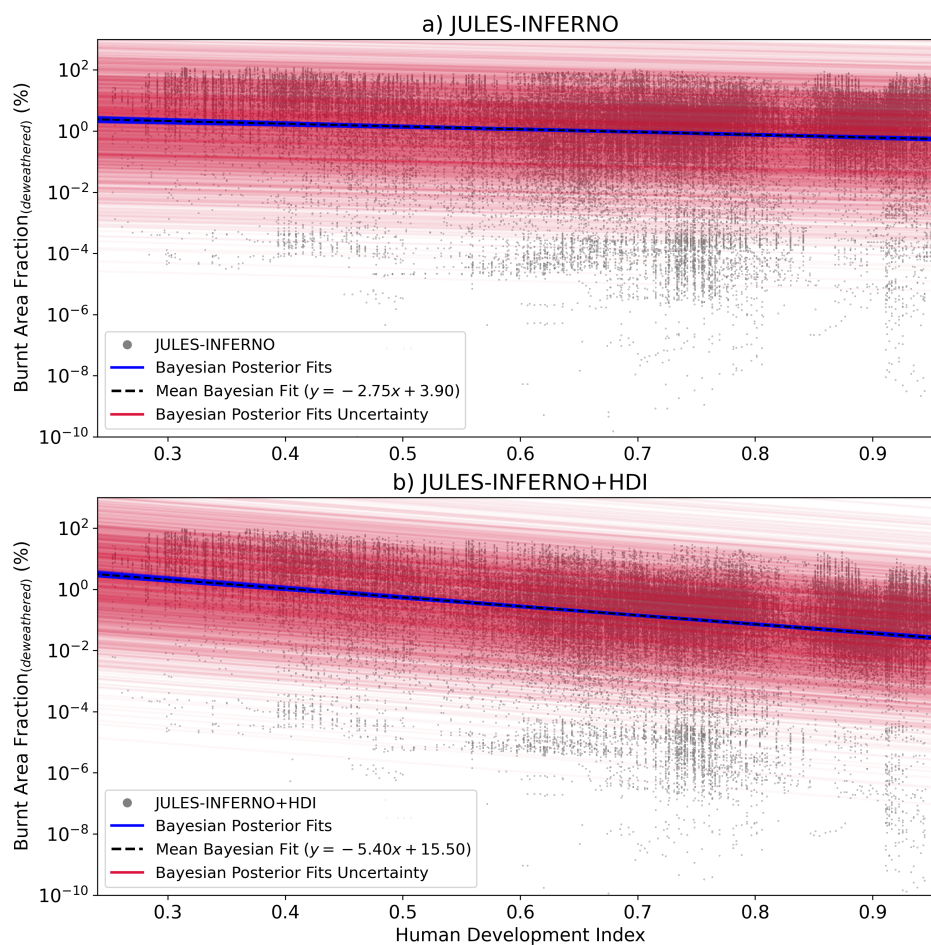


**Figure 6.** Relationship between the monthly mean (1997–2016) HDI and the log-transformed burnt area fraction (%) for (a) JULES-INFERNO and (b) JULES-INFERNO+HDI. The grey dots represent the burnt area fraction as a function of HDI. The blue solid lines indicate the Bayesian regression posterior fits, while the black dashed line shows the mean Bayesian fit. The red solid lines depict the uncertainty from the Bayesian posterior fit residuals.

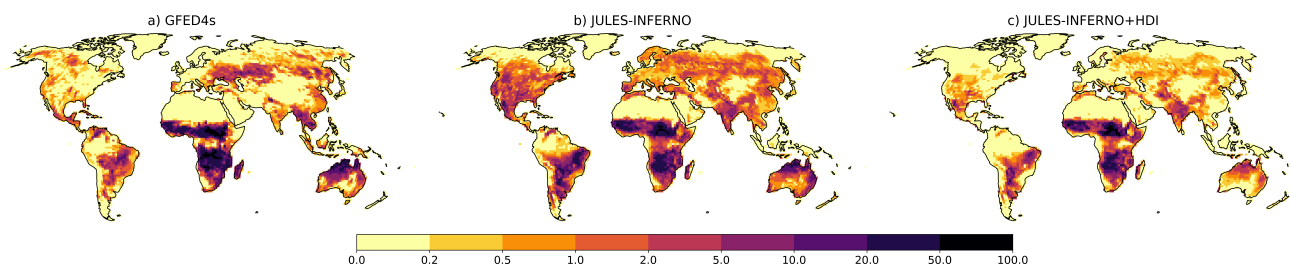


**Figure 7.** Burnt area fraction (%) mean annual average (1997 - 2016) for a) GFED4s, b) JULES-INFERNO and c) JULES-INFERNO+HDI. Please note that the colour mapping uses a colour axis in which the difference in colours do not correspond linearly to differences in burnt area fraction.

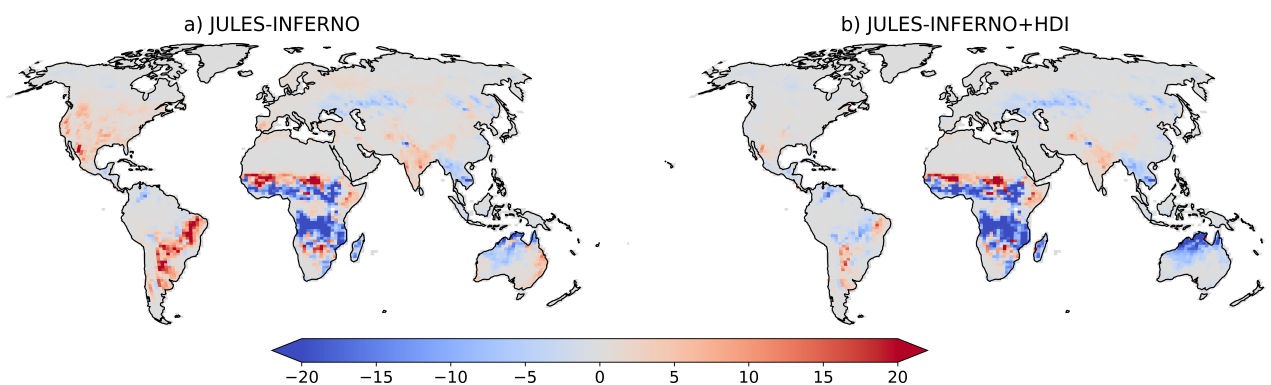


**Figure 8.** Burnt area fraction (%) mean annual average bias (1997 - 2016) for a) JULES-INFERNO, and b) JULES-INFERNO+HDI, calculated relative to the GFED4s observations

the positive bias over South America and India, although it increases the negative bias over the boreal regions, Australia, and South East Asia.

To further evaluate the impact of incorporating socio-economic factors on fire dynamics in INFERNO, we present histograms depicting the frequency distribution of burnt area across different fire regions in Figure 9. These histograms provide valuable insights into how the inclusion of socio-economic factors in JULES-INFERNO+HDI influences the occurrence of fires of different magnitudes compared to both JULES-INFERNO and GFED4s observations. This analysis helps to identify the dominant fire sizes in each region, assess whether the introduction of socio-economic factors leads to shifts in these distributions, and determine if the implementation in JULES-INFERNO+HDI leads to a better representations of the burnt area probability distribution.

Globally, GFED4s observations display a steep decline in burnt area frequency as fire sizes increase, with small burnt area fractions dominating the distribution. Both Both JULES-INFERNO and JULES-INFERNO+HDI exhibits an underestimation of the frequency of larger burnt areas in the range of 0.3 to 0.7. By incorporating HDI to represent these factors together with

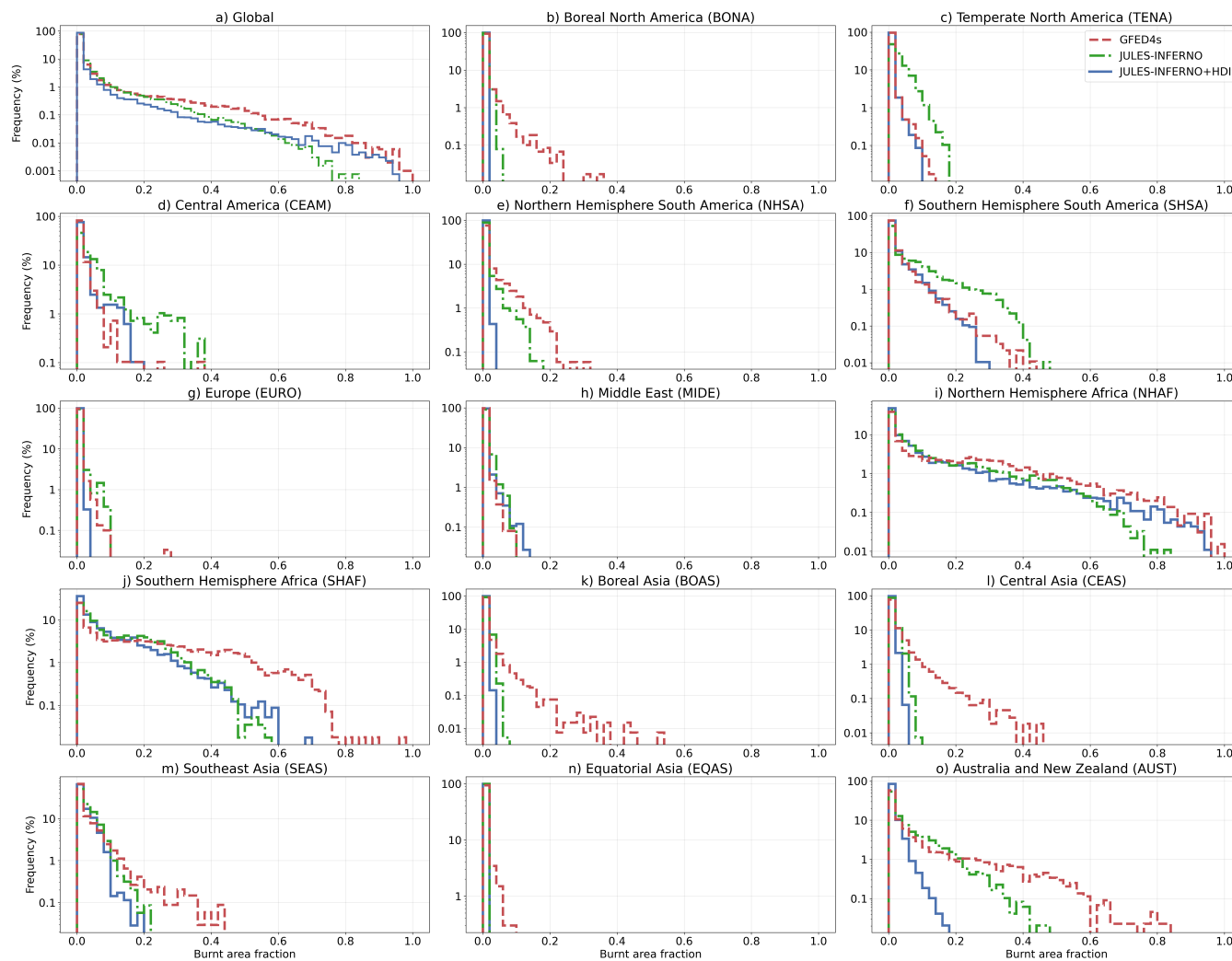


**Figure 9.** Histograms showing the distribution of burnt area fractions across fire regions for GFED4s observations (red dashed lines), JULES-INFERNO (green dotted lines), and JULES-INFERNO+HDI (blue solid lines), for the different fire regions.

revised parameters for  $\overline{BA_{PFT}}$ , JULES-INFERNO+HDI increases the frequency of large burnt areas, resulting in a distribution that more closely aligns with GFED4s, particularly for fire sizes between 0.7 and 1.0.

295 In boreal regions, Boreal North America (BONA) and Boreal Asia (BOAS), GFED4s observations show distributions dominated by smaller burnt areas, with a rapid decline in frequency as fire size increases. In contrast, both JULES-INFERNO and JULES-INFERNO+HDI under-represent moderate to large burnt areas, particularly above 0.1. This discrepancy suggests that both model configurations struggle to capture the fire dynamics typical of boreal environments. With the incorporation of HDI in JULES-INFERNO+HDI, the frequency of burnt areas is noticeably reduced, as a result of enhanced suppression introduced  
300 through HDI.

Temperate regions, such as Temperate North America (TENA) and Europe (EURO), exhibit fire dynamics characterized by a dominance of small burnt areas, with GFED4s showing a steep decline in fire frequency as fire size increases. JULES-INFERNO over-predicts the frequency of larger burnt areas in both regions, particularly above 0.1, highlighting the model's limitations in representing fire suppression. The introduction of HDI in JULES-INFERNO+HDI results in a marked reduction  
305 in the overestimation of large fires in TENA, improving the agreement with observations. In EURO, the inclusion of socio-economic factors better represents both small and moderate burnt area fractions, suggesting a more accurate reflection of the extensive fire suppression practices typical of developed regions.

In regions such as Central America (CEAM) and Southern Hemisphere South America (SHSA), GFED4s shows broader frequency distributions, with a more gradual decline in frequencies and significant contributions from small and moderate  
310 burnt areas. JULES-INFERNO strongly over-predicts burnt areas frequencies, particularly above 0.1, indicating an inadequate representation of fire suppression dynamics. JULES-INFERNO+HDI narrows this distribution, reducing the occurrence of large fires and better capturing the observed frequencies.

Northern Hemisphere Africa (NHAF) and Southern Hemisphere Africa (SHAF) are regions where the frequency of larger burnt areas is higher than in other regions according to GFED4s. Both model configurations underestimate large burnt areas,  
315 though JULES-INFERNO+HDI shows an improved representation by increasing the frequency of extreme fire sizes, particularly in NHAF.

For the Asian regions, such as Equatorial Asia (EQAS), Central Asia (CEAS), East Asia Asia (SEAS), Australia and New Zealand (AUST), GFED4s demonstrates a dominance of medium to small burnt areas. Both model configurations tend to under-predict medium fire sizes (e.g., between 0.2 and 0.6) when compared to observations, with JULES-INFERNO+HDI  
320 showing further increase of this negative bias, particularly in AUST.

By introducing a socio-economic representation of fire suppression, JULES-INFERNO+HDI reduces the frequency of large burnt areas in many regions, addressing overestimations in burnt area that were prevalent in the original JULES-INFERNO configuration. This improvement is particularly evident in regions such as TENA, CEAM, SHSA, and NHAF, where socio-economic factors are likely to play a critical role in fire management.

325 Nevertheless, discrepancies remain in some regions, such as NHSA, and AUST, where the model continues to under-predict medium and large fire sizes. These persistent biases suggest that while the inclusion of HDI represents a significant advance-



ment, further refinements in the socio-economic parametrization and consideration of other regional factors may be necessary to achieve more accurate fire size distributions regionally and globally.

JULES-INFERNO+HDI has a smaller bias than JULES-INFERNO at a regional scale, especially in regions where JULES-INFERNO presented large positive biases. However, the savanna regions in Africa, Australia, and central Eurasia are impacted negatively with negative biases increasing in JULES-INFERNO+HDI.

Figure 10 shows the burnt area annual mean time series. To assess the ability of the model simulations to reproduce the timeseries in comparison with observations, we perform a statistical analysis including the calculation of various metrics such as the Root Mean Squared Error (RMSE), Root Mean Squared Error after removal of a constant mean bias ( $RMSE_{UB}$ ), the bias, Pearson correlation, and Standard Deviation (STD) of the burnt area monthly and annual mean time series for all GFED4s regions (Table A1). We also assess the model's ability to reproduce observed trends using a simple log-transformed linear regression. Figure 11 summarises those statistical measures for both model configurations.

The results presented both in Figures 10 and 11 show that the inclusion of the socio-economic factors in INFERNO leads to improvements in the simulation of annual burnt area for regions such as Temperate North America (TENA), Central America (CEAM), Southern Hemisphere South America (SHSA), Europe (EURO), consequently reducing the large relative bias found in these regions in the experiments with JULES-INFERNO. This bias reduction is especially important for many areas with a substantially large relative bias (bias greater than 150 %) in JULES-INFERNO against observations.

For example, the bias in the TENA region is reduced from 735.6 % in JULES-INFERNO to 44.5 % in JULES-INFERNO+HDI. Other bias reductions include 259.22 % to 24.24 % in CEAM, 191.73 % to -1.72 % in SHSA, 258.81 % to -48.79 % in EURO, and 420.52 % to 231.75 % in MIDE. Conversely, there is a smaller, but still noteworthy, increase in the relative bias for NHSA from -60.06 % in JULES-INFERNO to -94.27 % in JULES-INFERNO+HDI, AUST from -21.79 % to -82.29 %, and SHAF from -45.27 % to -55.31 %.

Despite the socio-economic factors in INFERNO resulting in a reduction of bias and RMSE in regions where improvements are most needed, it also results in a general reduction in the interannual variability of the burnt area. Although this effect yields improvements in some regions, such as TENA and CEAM, including HDI tends to impact regions which experience high levels of burning negatively.

These results suggest that, although there is good agreement between the observed mean burnt area and JULES-INFERNO at a global scale (e.g., a bias of -7.21 %), this is due to compensating biases at the regional scale. We find that JULES-INFERNO+HDI performs better overall regionally, improving the representation of global burnt area variability ( $STD / STD_{GFED4s} = 0.99$ ; Table A1), reducing the global RMSE when the constant bias is removed ( $RMSE_{UB}$  is reduced from 32.50 in JULES-INFERNO to 24.12 in JULES-INFERNO+HDI), and leading to a higher global correlation with GFED4s (correlation of 75.25 % and 84.19 % for JULES-INFERNO and JULES-INFERNO+HDI respectively; Table A1). Nonetheless, JULES-INFERNO+HDI underestimates the global mean burnt area, resulting in a larger bias when compared to GFED4s.

The improvements from JULES-INFERNO+HDI in regions such as TENA, NHAF, and SHAF have a greater impact on the global metrics than the reduced performance seen for regions such as CEAM, NHSA, SHSA, EURO, and MIDE. For regions such as BOAS, CEADS, SEAS, EQAS, and AUST, both model configurations underperform in terms of standard deviation,

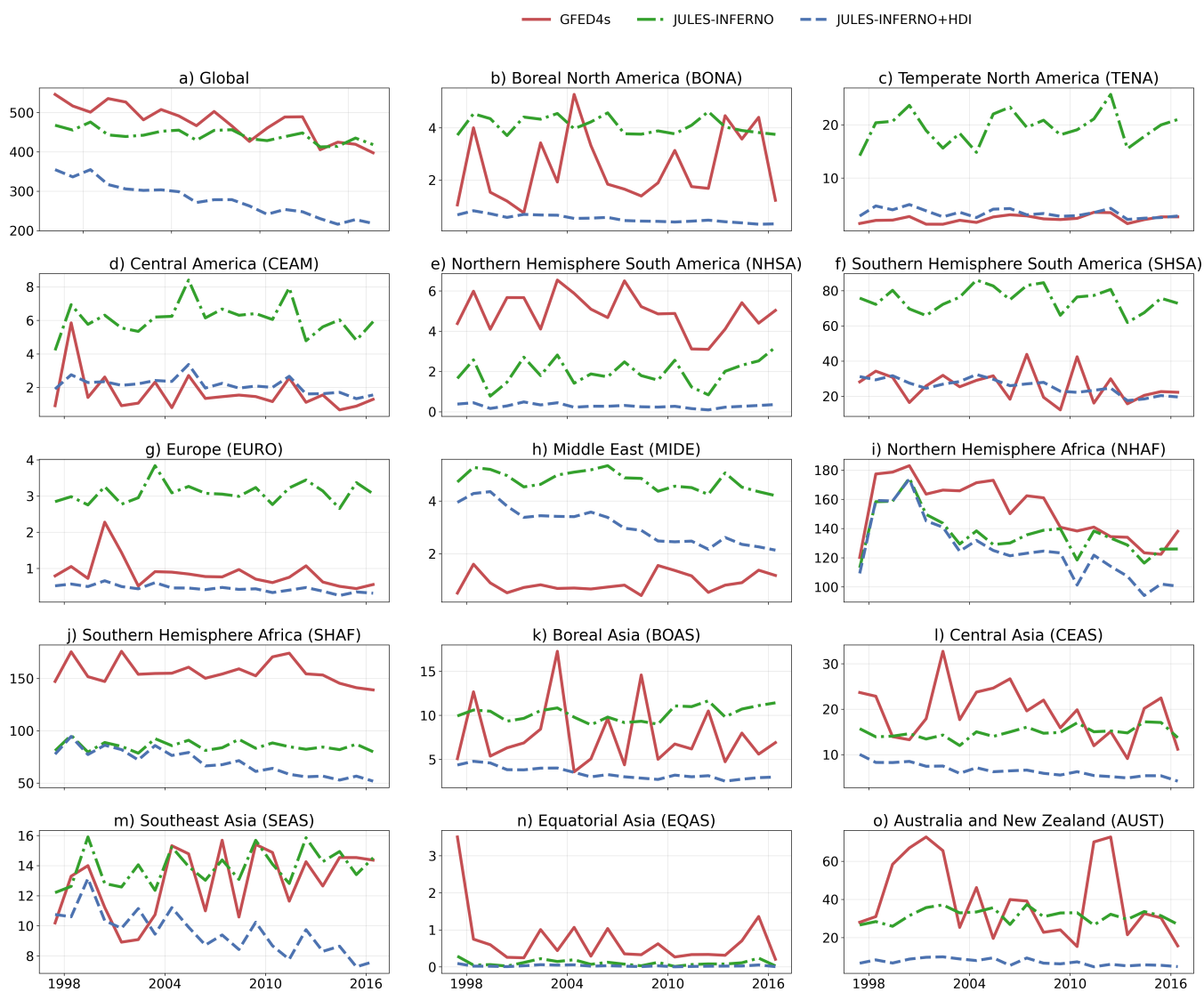


**Figure 10.** Time series of annual mean burned area (*Mha*) from 1997 to 2016 across different fire regions, shown for GFED4s (solid red line), JULES-INFERNO (green dot-dash line), and JULES-INFERNO+HDI (blue dashed line).

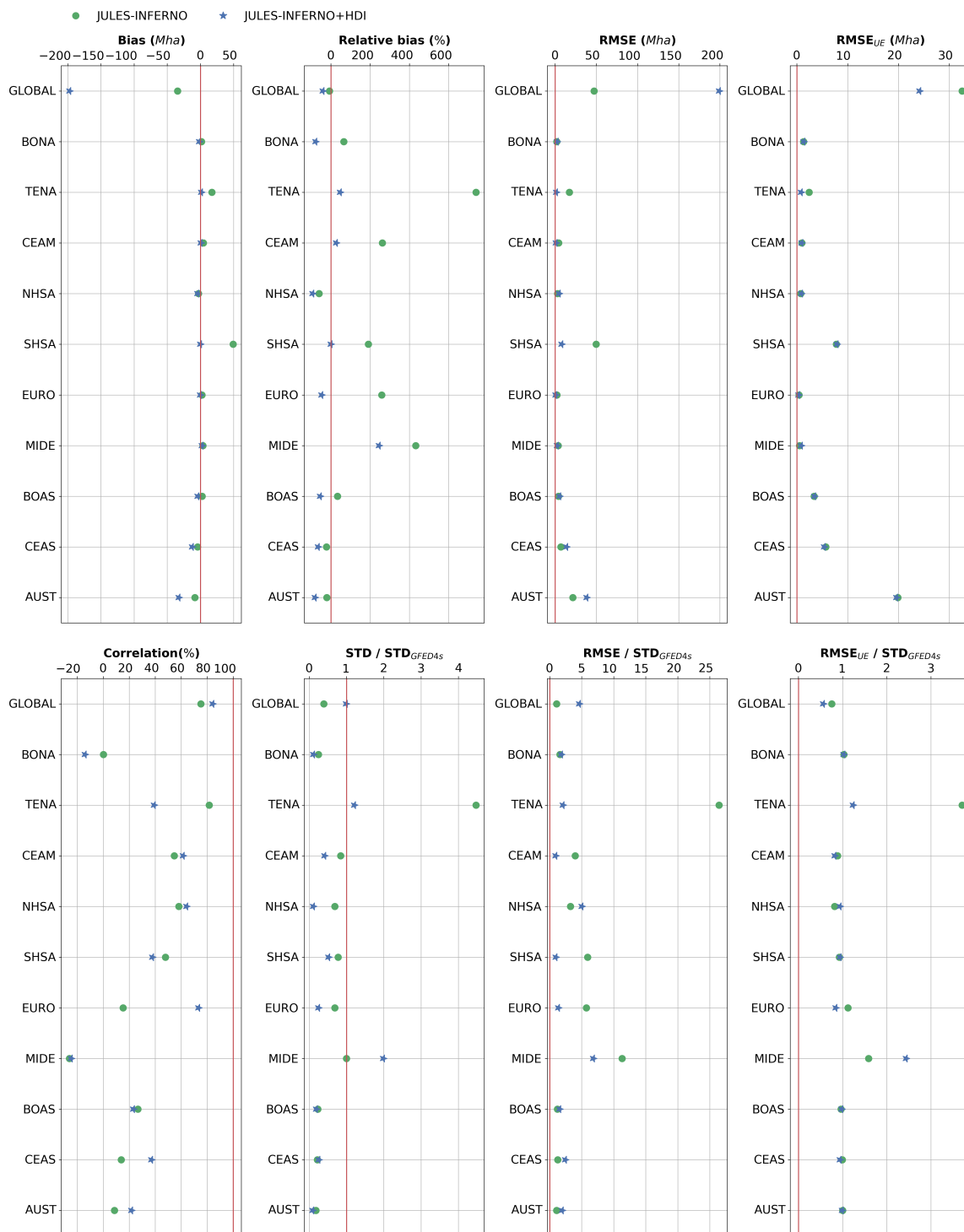


**Figure 11.** Summary of the statistics presented in Table A1 comparing JULES-INFERNO (green circle) and JULES-INFERNO+HDI (blue star). The red line show the reference value for a perfect simulation, the closer the experiment symbol is from this line the better.



and any differences between the  $STD / STD_{GFED4s}$  are small when compared to the observed standard deviation (e.g., difference between the JULES-INFERNO and JULES-INFERNO+HDI  $STD / STD_{GFED4s}$  smaller than 15 %).

365 Furthermore, for some of these regions INFERNO is not expected to agree well with observations, especially in terms of variability, as the fire behaviour of some of these regions is characterised by mechanisms that are not represented in INFERNO. This will be further discussed in Section 4.

### 3.3 Impact on burnt area trends

Including socio-economic factors in INFERNO adds a new external constraint to the model. Through this, historical changes to socio-economic factors influence how changes in population density affect fire ignitions in the model (see Section 2.2 and 370 Figure 4). Specifically, for regions with high HDI, variations in population have less of an impact on anthropogenic ignitions, while for regions with low HDI, variations in population can have a more considerable impact. This alters the importance of population density changes for highly developed regions, making HDI the dominant factor shaping burnt area trends.

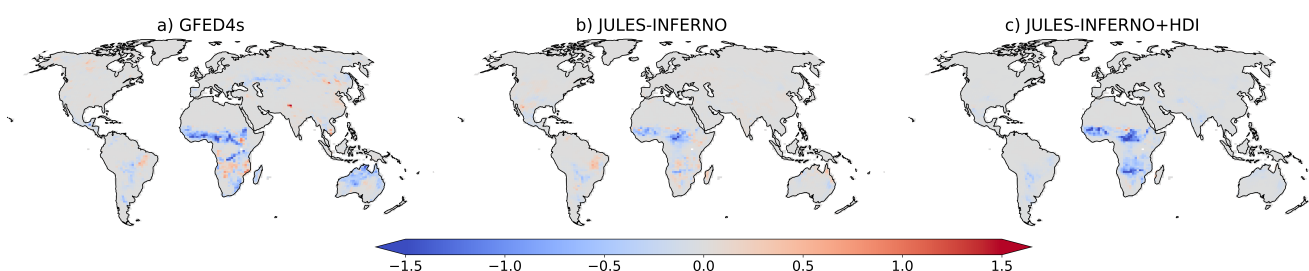


**Figure 12.** Burnt area fraction trend ( $\% \text{ year}^{-1}$ ) (calculated between the period 1997 - 2016) for a) GFED4s, b) JULES-INFERNO and c) JULES-INFERNO+HDI.

As shown in Figure 12, both JULES-INFERNO and JULES-INFERNO+HDI represent the main global burnt area trends. JULES-INFERNO is able to represent the regions with burnt area increases (e.g., Southern Africa and Northeast South America) and captures the dominant region for decreased burnt area - North Africa. However, this model setup tends to have weaker negative trends when compared to GFED4s. Conversely, JULES-INFERNO+HDI presents stronger trends, better representing those found in observations. However, it does not reproduce the positive trends in Southern Africa and Northeast South America. Both JULES-INFERNO and JULES-INFERNO+HDI are unable to represent the observed trends in Central Asia or Boreal North America.

380 Nonetheless, it should be noted that over the 2001–2012 period, Andela and Van Der Werf (2014) estimated that 51 % of the upward trend over southern Africa can be attributed to El Niño-Southern Oscillation (ENSO), while there is also evidence that socio-economic developments can be responsible for a decline. The relation between ENSO and annual burned area depends both on the effect of ENSO on precipitation and on the antecedent precipitation-burned area response. While the model setup is able to capture ENSO variability, as its weather is driven by reanalysis, there is no mechanism that allows INFERNO to 385 represent the antecedent precipitation-burned area effects due to litter build up. This is a limitation of the model and it should



not be expected for the model to perform well in regions where this precipitation-burned area coupling can be dominant, such as Central America, Northern Hemisphere South America, Europe, Northern Hemisphere Africa, and Central Asia (Andela et al., 2017; Abatzoglou et al., 2018).

Overall, including socio-economic factors in INFERNO results in an improvement in burnt area trends in comparison with  
390 observations. As seen in Table A1, JULES-INFERNO+HDI better represents the global negative trend in burnt area when compared to observations ( $-6.77 \text{ Mha year}^{-1}$  for GFED4s,  $-2.24 \text{ Mha year}^{-1}$  for JULES-INFERNO, and  $-7.58 \text{ Mha year}^{-1}$  for JULES-INFERNO+HDI). This improvement comes mostly from a better representation of the burnt area trends in regions with strong negative trends, such as SHSA, NHAf, CEAS and AUST, but also by better representing regions with weak negative burnt area trends, namely CEAM, NHSA, EURO and BOAS. Moreover, in regions such as CEAM, NHSA, EURO, BOAS,  
395 CEAS, and AUST, JULES-INFERNO+HDI shows a negative burnt area trend, in better agreement with observations.

Contrary to these improvements, JULES-INFERNO+HDI can also produce trends that are too strong. For example, for Southern Hemisphere Africa (SHAF), although JULES-INFERNO+HDI has the same burnt area trend sign as in the observations (negative), the trend is too strong ( $-0.54 \text{ Mha year}^{-1}$  for GFED4s,  $-0.14 \text{ Mha year}^{-1}$  for JULES-INFERNO, and  $-1.94 \text{ Mha year}^{-1}$  for JULES-INFERNO+HDI), and JULES-INFERNO provides a better representation in these regions. In  
400 addition, for regions where observations show a positive burnt area trend (TENA, MIDE and SEAS), JULES-INFERNO+HDI has a trend of opposite sign (negative). At the same time, JULES-INFERNO can capture the positive trend in TENA and SEAS.

Nonetheless, the observed dataset (GFED4s) shows that out of 14 regions, four have positive burnt area trends (Table A1). JULES-INFERNO only presents a positive trend for TENA and SEAS. While JULES-INFERNO+HDI tends to enforce decreasing trends, this only happens in four regions out of 14 (i.e., TENA, SHAF, MIDE, and SEAS). For the remaining 10  
405 regions, JULES-INFERNO+HDI presents a similar trend to JULES-INFERNO or even an improved trend when compared to GFED4s.

It should be noted that, in some of these regions INFERNO does not model all the processes that represent fire behaviour. This has an impact on overall model results. For example, due to the typical model resolution and timescales in Earth System Modelling, INFERNO was not designed to model the processes and mechanisms that are needed to represent large and severe  
410 fires which dominate the trends and fire regime characteristics of these regions. Therefore, it is expected that regions where fire regimes are dominated by large and severe fires may be affected by a negative bias in burnt areas and fire emissions, as well as on their response to a changing climate.

### 3.3.1 Impact of external model drivers on burnt area trends

As described in section 2.3, the JULES-ES experimental setup relies on ancillary forcing data to represent external processes  
415 to JULES, such as atmospheric weather conditions, atmospheric composition, population density, and biogenic drivers. These external forcings can drive fire by forcing changes to the evolution of land surface properties, fire ignitions, and fire weather. It is important to understand the impact these external drivers have on the burnt area trends and the interaction with the parametrised socio-economic factors in fires. Therefore a set of sensitivity experiments was performed by fixing the external model drivers to the year 1990 and only allowing an individual external driver to vary transiently through the experiment.



- 420 – **1990 control:** where all external model drivers are fixed to year-1990 values
- **clim:** where only the atmospheric drivers are transient (downward longwave radiative flux, downward shortwave radiative flux, precipitation, surface pressure, air temperature, meridional and zonal wind components)
- **tas:** where only air temperature at 2 m is transient
- **ppn:** where only precipitation is transient
- 425 – **lu:** where only the land use is transient
- **Ndep:** where only Nitrogen deposition is transient
- **pop:** where only population density is transient
- **CO<sub>2</sub>:** where only the atmospheric carbon dioxide (CO<sub>2</sub>) mixing ratio is transient
- **HDI:** where only the Human Development Index is transient (only for JULES-INFERNO+HDI)

430 These sensitivity experiments branched from their respective control runs - JULES-INFERNO and JULES-INFERNO+HDI - starting from 1990 and run up to 2016. In this way, the underlying land surface state from the reference run is preserved, and only changes to the forcing that take place during the period of interest are taken into effect. The trends for each relevant external forcing are in Supplementary Figure A3.

The results of these sensitivity experiments on the burnt area trends ( $Mha\ year^{-1}$ ), and respective standard error, for the  
435 different GFED4s fire regions are presented in Table A2 in the Appendix for JULES-INFERNO and Table A3 for JULES-INFERNO+HDI. These results are summarised in Figure 13. Burnt area trends in JULES-INFERNO tend to be driven by climate, land use, or population density changes (relative contribution greater than 50 % when compared to their reference), with the dominant driver (the sensitivity experiment with the largest absolute trend value) for the majority of regions being climate (including through air temperature and precipitation), for example, BONA, TENA, NHSA, SHSA, EURO, MIDE,  
440 SHAF, BOAS, CEAS, SEAS, and AUST. On the one hand, air temperature is a dominant, and statistically significant, driver of increasing burnt area trends for CEAM, NHSA, BOAS and CEAS. For MIDE, precipitation has a dominant role in reducing burnt area. On the other hand, despite dominating the burnt area trends, temperature and precipitation can have opposite effects. Namely, for BONA (not significant for air temperature), TENA, SHSA, EURO, and AUST, precipitation causes a reduction in burnt area, while temperature results in an increase, although results are not statistically significant for precipitation over  
445 TENA, SHSA, EURO, CEAS, CEAM and AUST.

Anthropogenic drivers, such as land use and population density can play a major role in some regions. For example, land use is the dominant driver in SHSA and SHAF, population density in CEAM, and both are important drivers in TENA, EURO, MIDE, NHAF. Land use can cause either an increase (TENA, EURO, and SHAF) or a decrease in burnt area, while population density results in a reduction in burnt area for all the regions where this external driver is dominant (TENA, CEAM, EURO,  
450 MIDE, and NHAF).

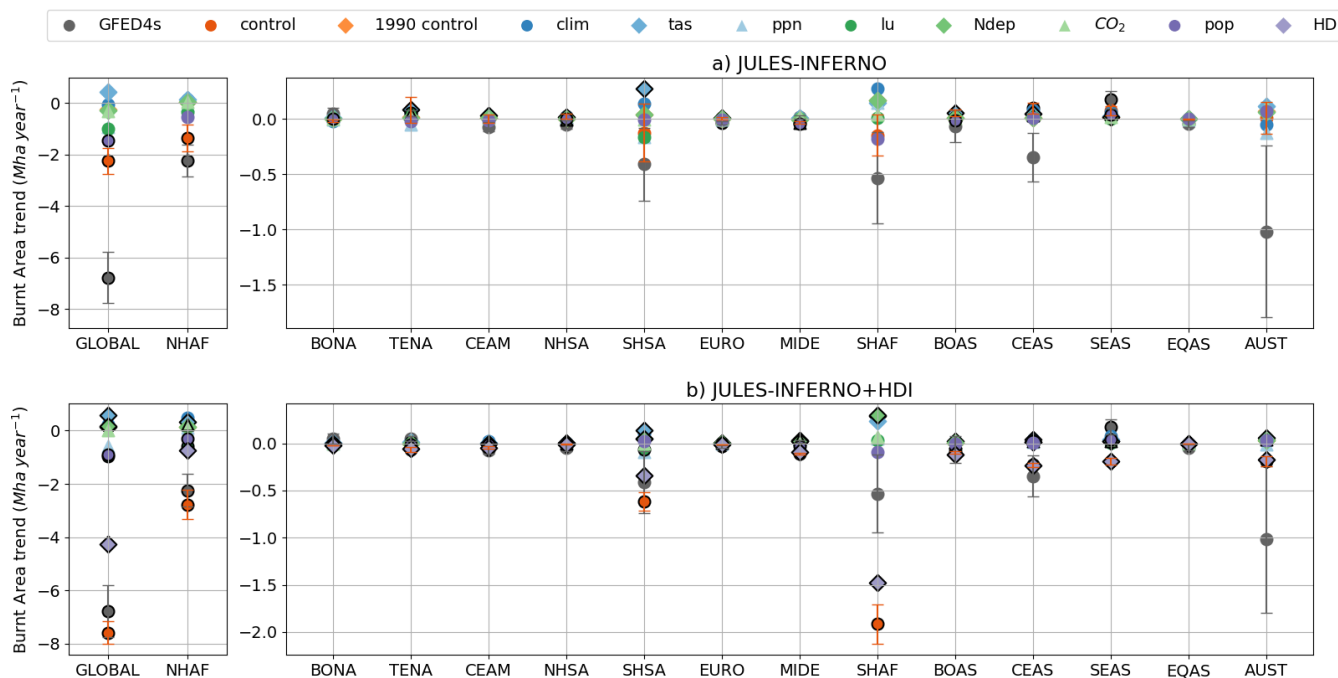


**Figure 13.** Burnt area trends ( $Mha\ year^{-1}$ ) for the different GFED4s fire regions (Giglio et al., 2013) from the model sensitivity experiments for a) JULES-INFERNO and b) JULES-INFERNO+HDI. The whiskers for the values of GFED4s and *control* represent the standard error associated with the trend. Markers whose edge is coloured in black represent trends that are significantly different from zero at the 99 % confidence level. GLOBAL and NHAF regions are presented in separate panels to improve readability, due to their large trends compared to other regions.

Biogenic drivers such as nitrogen deposition and atmospheric carbon dioxide assimilation tend to play a less significant role in the burnt area trends, impacting burnt area trends only for NHSA through carbon dioxide, and CEAS through both nitrogen deposition and atmospheric carbon dioxide.

For JULES-INFERNO+HDI, HDI is the dominant factor in the burnt area trend for all regions, with the exception of NHAF and EQAS. This is evident in the sensitivity experiments for JULES-INFERNO+HDI where only HDI forcing is made transient (HDI). In all cases, including socio-economic factors in INFERNO changes the relative role that external forcings have in determining burnt area trends. For example, it reduces the role that climate, population density, and land use have in burnt area trends towards a stronger role from socio-economic effects (HDI).

This impact is especially evident when comparing the role of the climate forcing in driving burnt area trends between JULES-INFERNO and JULES-INFERNO+HDI in their respective sensitivity experiments, *clim*, *tas*, and *ppn*. For instance, for regions where temperature effects on burnt area trends were dominant in JULES-INFERNO, they show less of an impact from temperature in JULES-INFERNO+HDI, albeit still at a statistically significant level (e.g., TENA, EURO, CEAS, and AUS). In addition, where the climate contributions to the burnt area trends were small in JULES-INFERNO (BONA, CEAM, and NHSA),



when considering socio-economic factors, these become statistically non-significant in terms of the climate contributions to the  
465 trends. In addition, including socio-economic factors in INFERNO leads to a change in how precipitation and temperature can  
impact some regions. For example, precipitation was the dominant driver of burnt area trends in JULES-INFERNO for MIDE,  
causing a reduction of burnt area (trend of  $-0.038 \text{ Mha year}^{-1}$ ). Conversely, in JULES-INFERNO+HDI, precipitation has less  
impact on the burnt area trend (trend of  $-0.016 \text{ Mha year}^{-1}$ ), while temperature has a larger impact on the burnt area trend  
( $+0.034 \text{ Mha year}^{-1}$ ). A similar result is also seen for NHAf, where the role of temperature becomes statistically signifi-  
470 cant in JULES-INFERNO+HDI (trend of  $+0.342 \text{ Mha year}^{-1}$ ), while it was not statistically significant in JULES-INFERNO  
(trend of  $+0.007 \text{ Mha year}^{-1}$ ).

Moreover, results show a difference in the role of anthropogenic drivers (land use and population density) on burnt area trends  
between JULES-INFERNO and JULES-INFERNO+HDI sensitivity experiments. For BONA, CEAM, and NHAf regions,  
burnt area decreases for JULES-INFERNO+HDI (*pop* and *lu*) sensitivity experiments while for JULES-INFERNO (*pop* and  
475 *lu*) an increase was simulated.

Together, these results show that including socio-economic factors in the representation of fires in Earth System Models is  
important for simulating the burnt area mean state, for quantifying burnt area trends and for understanding the main drivers of  
those trends at regional scales.

#### 4 Discussion & Conclusions

480 This work aims to represent socio-economic factors, through the use of the HDI, together with the Pechony and Shindell (2009)  
anthropogenic fire ignitions to parameterise human socio-economic impacts on fires. When using the INFERNO fire model,  
the aim was to improve the regional representation of human–environmental coupling for applications at large spatial scales  
within an ESM.

The results presented in this study show that including socio-economic factors in the fire ignition and suppression parametri-  
485 sation within INFERNO together with revised  $\overline{BA_{PFT}}$  parameters, leads to an improved representation of the relationship  
between burnt area and HDI, as found in observations - Figures 3 and 6 - leading in turn to improvements in performance in  
regions that were affected by large positive biases in the JULES-INFERNO configuration.

The simple representation of HDI captures how more complex socio-economic processes tend to suppress fires as devel-  
opment increases. The observed linear relationship between burnt area and HDI suggests that regions with higher HDI tend  
490 to have lower average values of burnt area. This trend can be attributed to various components of HDI that influence govern-  
ment policies and resources for fire management (Miranda-Lescano et al., 2023). For instance, the gross national income index  
indicates that higher HDI regions typically have more funding available for fire prevention and suppression efforts (Rideout  
et al., 2017). Similarly, the life expectancy index suggests that these governments are more likely to implement policies aimed  
at mitigating the negative impacts of fire on their population (Rizzo and Rizzo, 2024). Additionally, the education index high-  
495 lights that educational initiatives can enhance community awareness and preparedness regarding fire risks and environmental  
stewardship (Prestemon et al., 2010). Collectively, these factors help explain the observed trend and underscore the utility of



HDI as a general proxy for representing socio-economic influences in fire management, but may not be fully representative of specific particularities of any single given region.

Large bias reductions are evident in Temperate North America (TENA), Central America (CEAM), Southern Hemisphere South America (SHSA), Europe (EURO), and Middle East (MIDE), with the largest reductions in TENA where a 735.57 % bias in JULES-INFERNO is reduced to 44.46 % in JULES-INFERNO+HDI. It should be noted that for Australia and New Zealand (AUST) and East Asia (SEAS), JULES-INFERNO+HDI performance is reduced, increasing the negative bias when compared to INFERNO-JULES. Furthermore, it should be highlighted that although JULES-INFERNO performs well at the global scale, as can be seen when comparing the annual mean burnt area against GFED4s in Figure 11, this is due to compensating errors at the regional level.

The histograms of burnt area frequency across different fire regions, Figure 9, reveal key differences in how fire sizes are distributed between JULES-INFERNO, JULES-INFERNO+HDI, and GFED4s observations. The implementation of HDI resulted in notable improvements in regions such as Temperate North America (TENA), Central America (CEAM), Southern Hemisphere South America (SHSA), and Northern Hemisphere Africa (NHAF). In these regions, the reduction in the frequency of large burnt areas suggests that including socio-economic factors better captures the dynamics of fire suppression associated with higher levels of human development and management practices. However, discrepancies against observations remain in JULES-INFERNO+HDI for regions such as Northern Hemisphere South America (NHSA), and Australia and New Zealand (AUST), where the model continues to underpredict medium and large fire sizes.

Moreover, including socio-economic factors in INFERNO-JULES+HDI improves the representation of the burnt area trends, especially in areas where GFED4s presents negative trends. At the same time, JULES-INFERNO shows no significant trends (e.g., SHSA, NHAF, CEAS, and AUST), as well as better representing regions with weak negative burnt area trends (CEAM, NHSA, EURO, and BOAS). However, JULES-INFERNO+HDI can also produce overly strong trends (e.g., SHAF) or misrepresents the observed positive burnt area trends found in TENA, MIDE and SEAS.

As mentioned previously, observations (GFED4s) show that out of 14 regions, four have a positive burnt area trends. From these, only JULES-INFERNO shows a positive trend for TENA and SEAS. While JULES-INFERNO+HDI tends to strengthen decreasing trends, this only happens in four regions out of 14 (TENA, SHAF, MIDE, and SEAS). For the remaining 10 regions, JULES-INFERNO+HDI shows a similar trend to JULES-INFERNO or even an improved trend when compared to GFED4s.

It should be highlighted that in some of these regions, INFERNO does not model all of the processes that impact fire behaviour. This has an impact on overall model results. For example, INFERNO was not designed to capture the dynamics of large, severe fires that dominate fire regimes in some regions. As a result, these areas may show a negative bias in burned area and fire emissions, as well as in their response to climate change.

Overall, the improved representation of the burnt area trends in JULES-INFERNO+HDI when compared to JULES-INFERNO highlights the importance of including the socio-economic factors in fire ignition and suppression in order to better reproduce the observed fire trends. This impact is especially evident when comparing the role of external climate drivers on burnt area trends between JULES-INFERNO and JULES-INFERNO+HDI using a set of sensitivity experiments. The results of these



experiments show that including socio-economic impacts on fire results in the burnt areas trends being dominated by socio-economic drivers through a reduction in the contribution from climate drivers, especially from temperature and precipitation.

#### 4.1 Modelled burnt area trends

We have shown that introducing the representation of socio-economic factors can change the impact external forcing has on burnt area trends and that the mechanisms that lead to this can differ at a regional level. For example, the inclusion of socio-economic factors reduces the role of temperature in driving trends (e.g., increase for TENA, EURO, CEAS, and AUS), as well as by changing the behaviour that climate drivers have in burnt area trends (e.g., MIDE, NHAF, and SEAS). Socio-economic factors also alter the influence of land use and population density, increasing their impact on fire activity by shaping how human activity interacts with fire regimes. (e.g., BONA, CEAM, and NHSA).

Although HDI does not encompass explicitly the impacts of fire management policies, these results are consistent with other studies, which show that for developed regions, land and fire management policies have a greater role than other human behaviours in controlling ignitions (Nikolakis and Roberts, 2022; Ford et al., 2021; Jacobson et al., 2022; Carreiras et al., 2014; Mourão and Martinho, 2014).

The work of Kelley et al. (2019) and Jones et al. (2022) shows that, despite the increases in fire weather seasons and fire weather extremes that have been observed in all world regions, burnt area has shown a variety of regional trends and that the negative trends were found to be significant only in Africa (NHAF and SHAF), Europe (EURO), and Central Asia (CEAS). At a global scale, burnt area trends show a decline predominantly driven by a decline in burnt area in the savannah-grassland systems caused by the expansion of high-capital agriculture (Andela et al., 2017), as well as reductions in vegetation productivity driven by changes to the hydrological balance (Zubkova et al., 2019). The results on the impact of external model drivers on burnt area trends, detailed in Section 3.3.1, agree with this. In both JULES-INFERNO and JULES-INFERNO+HDI, the dominant factor contributing to the negative trend in global burnt area are linked to anthropogenic drivers (land use, population density and HDI), as well as precipitation. Several authors have also shown that declines in burnt area in the Mediterranean have occurred irrespective of increases in fire weather, as well as extensions to the fire weather season length, which is attributed to increased fire prevention and in combating and mitigating fire impacts (Jones et al., 2022; Urbietta et al., 2019; Carreiras et al., 2014; Mourão and Martinho, 2014).

Moreover, results show the impact of the anthropogenic drivers (land use and population density) have in the burnt area trends, resulting in a decrease in burnt area for JULES-INFERNO+HDI compared to JULES-INFERNO, for BONA, CEAM, and NHSA regions. This result, combined with the impact seen in the reduction of the effects temperature has in burnt area, are especially relevant in South America (NHSA and SHSA), leading to a better performance of JULES-INFERNO+HDI in these regions overall. The impact of socio-economic effects on fire is also documented for the Amazonia region, where fire is routinely used for land clearing, resulting in a strong link between burnt area and deforestation rates. Through the last decade, this region has seen a decline in deforestation rates leading to an observed negative trend in burnt area. However, this decline in burnt area has not been uniform due to historical shifts in economic and environmental policies (Silva Junior et al., 2021; Aragão et al., 2018; Nepstad et al., 2014).



565 The analysis of the impact of including socio-economic factors in INFERNO has also shown that JULES-INFERNO+HDI can also producing overly strong negative trends resulting in worse performance when compared to JULES-INFERNO (e.g., SHAF). In addition, for regions where observations present a positive burnt area trend (TENA, MIDE and SEAS), JULES-INFERNO+HDI presents an opposite trend sign (negative), while JULES-INFERNO is able to capture the positive trend in TENA and SEAS.

570 It is known that there is an increase in the frequency of large and severe fires in Continental United States of America (Goss et al., 2020; Williams et al., 2019; Abatzoglou and Williams, 2016), as well as boreal regions (Canada and Alaska) (Kasischke and Turetsky, 2006; Stocks et al., 2002; Veraverbeke et al., 2017), leading to observed increases in burnt area, with fire activity having a strong relationship with fire weather in these regions. However, INFERNO has been developed for Earth System Modelling resolutions and timescales, and it is not expected to be able to capture the representation of the processes that drive large and severe fires which dominate the trends and fire regime characteristics of these regions (e.g., it is based on the use of a value for the average burnt area for each plant functional type). Therefore, it is expected that regions where fire regimes are dominated by large and severe fires may be affected by a negative bias in burnt areas and fire emissions, as well as on their response to a changing climate.

#### 4.2 Model limitations and known issues

580 The use of socio-economic factors in INFERNO reduces the inter-annual variability of burnt area for most of the fire regions (Figure 10). While this improves INFERNO performance over regions such as TENA and CEAM, it results in a reduction in the variability overall, reducing the ability of the model to represent the burnt area regions that are characterised by high inter-annual variability, namely, BONA, BOAS, AUST, CEAS, SHSA and NHSA. Although this could be seen as a negative impact, it must be noted that the control model - JULES-INFERNO - despite having a larger inter-annual variability, also underperforms in this aspect compared to observations.

Although socio-economic factors are included in JULES-INFERNO+HDI, the HDI dataset provides information mainly at a national level. To improve the impact of socioeconomic activities on fire at a regional level, it would be beneficial to use data capturing the HDI changes at a sub-national administrative level. Furthermore, it should be highlighted that the HDI does not account for the different implementation of fire management practices and government policies at the regional level.

590 Another limitation in the representation of fires in INFERNO is the lack of a peat-burning in the model simulations described here. The work of Teixeira et al. (2021) highlights that this could be responsible for the negative bias over equatorial Asia and boreal regions where peatland fires represent a significant amount of burnt area and biomass burning emissions. Recent developments from Blackford et al. (2024) could significantly improve the model performance over these regions and help to reduce the burnt area bias both at regional and global scales.

595 In addition, biases in the underlying vegetation can significantly impact modelled burnt area. The work by Teixeira et al. (2021) is a good example of this. In their work, the authors show that although the burnt area fraction over Africa is well represented, there is a large (50 %) underestimation of the fires in the northern African region (NHAF). This underestimation is attributed to the Saharan bare soil extending too far south, causing a lack of grassland in the Sahel region, which is a result



of precipitation deficits associated with errors in the position and intensity of monsoon systems (Sellar et al., 2019b; Williams  
600 et al., 2018).

Despite the improvements introduced by Burton et al. (2019) to JULES, including fire-vegetation interactions, there are still  
a number of regions that show significant vegetation biases, which in turn affect the performance of INFERNO. For example,  
it is known that JULES vegetation has few needle-leaf trees across the boreal regions compared to observations.

These results highlight that the high burnt area variability in these regions may result from a mechanism not currently rep-  
605 resented in INFERNO. For example, Kirillina et al. (2020); Andela and Van Der Werf (2014) show how changes in areas with  
increasing anthropogenic alteration, such as agricultural systems, and changes in fire management practices and government  
policies, often lead to shifts in peak fire activity for regions such as India and southwest Russia. They also show that the  
widespread adoption of Aboriginal fire management with increased prescribed burning has curbed the frequency of large fires  
over a broad region in Australia. Similarly, the dominant spatial and temporal variability in the burnt area for Southern Europe  
610 and North Africa (Chergui et al., 2018), as well as South America (Chuvienco et al., 2021), is known to be driven by shifts in  
the amounts of fuel and continuity imposed by changes in socioeconomic drivers.

### 4.3 Concluding remarks

Socio-economic policies on management and control of fire play a major role in controlling fire ignition and suppression  
(Nikolakis and Roberts, 2022; Ford et al., 2021; Jacobson et al., 2022; Carreiras et al., 2014; Mourão and Martinho, 2014).  
615 This is especially important in the context of future climate projections (Pivello et al., 2021; Duane et al., 2019; Gillson et al.,  
2019; Paveglio et al., 2018). It is only with the understanding of the expected impact of climate change that adaptation and  
mitigation policies can be developed with the aim of protecting infrastructure and ecosystems from fire hazards. This shows the  
importance of representing socio-economic controls on fire when modelling future projections in an Earth System Modelling  
context.

620 This study shows that including a parametrisation for socio-economic impacts on fire based on HDI in INFERNO provides  
a simple and linear representation of these effects on fire ignition and suppression. This leads to an improvement in model  
performance, especially in developed regions.

Introducing socio-economic factors into INFERNO, reduces compensating biases and improves the modelled burnt area  
trends in comparison with observations. In particular, the results here show that including socio-economic factors in the rep-  
625 resentation of fires in Earth System Models is important for realistically simulating the burnt area mean state, for quantifying  
burnt area trends in the recent past, and for understanding the main drivers of those trends at regional scales.

The improvements JULES-INFERNO+HDI has in regions such as TENA, NHAF, and SHAF have a greater impact in the  
global metrics than the reduced performance seen for regions such as CEAM, NHSA, SHSA, EURO, and MIDE. For regions  
such as BOAS, CEADS, SEAS, EQAS, and AUST, both model configurations underperform in terms of standard deviation and  
630 any differences between the  $STD / STD_{GFED4s}$  are small when compared to the observed standard deviation (e.g., difference  
between the JULES-INFERNO and JULES-INFERNO+HDI  $STD / STD_{GFED4s}$  smaller than 15 %).



For regions such as NHSA, BOAS, CEAS, and AUST there is an increase in the bias introduced. However, it should be noted that these model limitations and known issues are discussed in Section 4.2 where the limitations of the model are highlighted and related to fire mechanisms that are not represented in INFERNO, or bias in the underlying vegetation model causing impacts on the modelling of fires.

Finally, the recent work by Perkins et al. (2024), proposes an alternative methodology for representing human influences in INFERNO. While the WHAM! framework introduced by Perkins et al. (2024) offers a more comprehensive approach, its increased complexity may present challenges in implementation within an ESM context. In contrast, the method presented in this study is straightforward and is directly applicable within the existing modelling framework of JULES-INFERNO for ESM.

Considering this, we recommend that socio-economic factors should be included in all fire modelling studies at both global and regional scales, particularly when considering future climate change scenarios. This work will form the basis of a future study on understanding the impact of fires in the Earth System when considering future climate change scenarios.



## Appendix A

### A1 Observed Datasets

#### 645 A1.1 The Human Development Index dataset

HDI originated from the annual Human Development Reports created by the United Nations Development Programme (UNDP) Human Development Report Office. These reports had the explicit purpose of shifting the focus of development economics from national income accounting to people-centred policies. The aim was to provide a simple composite measure of human development to convince the public, academics, and politicians to evaluate development not only by economic advances but  
650 also improvements in human well-being. HDI serves as a crucial metric for assessing the development status of regions globally, and it has been used in several studies to better understand the socio-economics impacts in the Earth System (ES) (Türe, 2013; Hickel, 2020; Roy et al., 2023).

HDI is a composite index (ranging from zero to one) measuring four key metrics (Bhanojirao, 1991):

- life expectancy at birth
- 655 – expected years of schooling
- average years of schooling
- gross national income (GNI) per capita

These metrics are then normalised by their respective maximum value, and HDI is calculated as the geometric mean of life expectancy, education, and GNI per capita, as shown in Eq. A1.

$$660 \quad HDI = (H_N \cdot E_N \cdot I_N)^{\frac{1}{3}} \quad (A1)$$

where  $H_N$  is the normalised life expectancy,  $E_N$  is the normalised arithmetic mean of the two education indices and  $I_N$  is the normalised GNI.

The work conducted by Kummu et al. (2018) introduces gridded global datasets for Gross Domestic Product (GDP) and Human Development Index (HDI), covering a 25-year period from 1990 to 2015 with annual frequency and a spatial resolution  
665 of 5 arc-minutes. This temporal coverage and high-resolution global scope enable comprehensive analyses of trends, patterns, and changes in HDI across diverse regions and timescales.

To produce these datasets, Kummu et al. (2018)s employed a comprehensive approach. For GDP, they utilized both sub-national and national-level data sources. Sub-national GDP data was derived from previous research, while national-level data was sourced from reputable institutions such as the World Bank and the Central Intelligence Agency World Factbook. The  
670 HDI dataset was compiled by initially constructing a full national HDI dataset based on data from the Human Development Reports by UNDP. For countries not included in the UNDP reports, independent data sources were utilized, and for missing or outdated data, a methodology involving scaled regional data was adopted.



## A1.2 Burnt Area observation

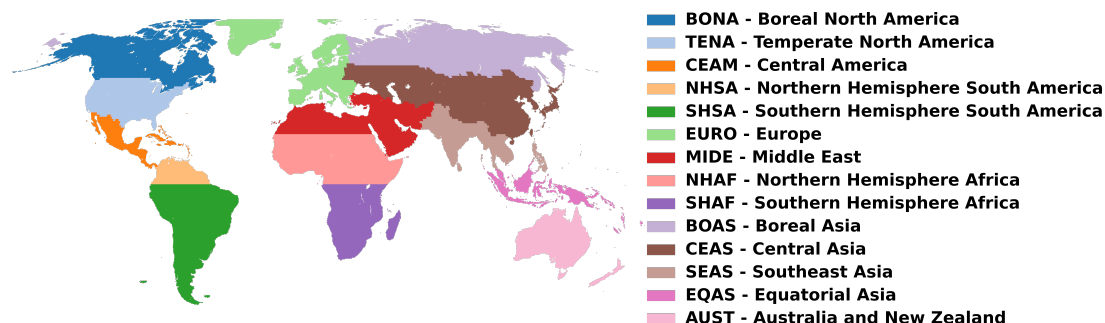


**Figure A1.** Basis regions, as defined in the GFED4s dataset (Giglio et al., 2013).

We use data from the Global Fire Emission Database version 4 (GFED4s) (Giglio et al., 2013) to understand the relation  
675 between HDI and burnt area, as well as to assess the model performance in simulating burnt area. This dataset is provided as a  
gridded product at a  $0.25^\circ$  resolution. It is derived from a multi-sensor satellite dataset, including satellite data based on active  
fire detection, and including small fires based on statistical modelling, as detailed in (Randerson et al., 2012). We apply regions  
defined in the GFED4s dataset to the modelled data to evaluate the results at a regional level (Figure A1).

## A1.3 Fire Weather Index

680 The work developed by Vitolo et al. (2020) provides an ERA5-based global meteorological wildfire danger dataset based on  
the Global ECMWF Fire Forecast (GEFF) model and the ERA5 reanalysis.

In this dataset the FWI is calculated using meteorological variables (e.g., such as temperature, humidity, precipitation, and  
wind speed) driven by the ERA5 reanalysis dataset. To accurately represent wildfire conditions at local noon, when fire danger  
is typically highest, atmospheric fields from ERA5 undergo preprocessing, stitching together hourly forecasts, ensuring that  
685 meteorological conditions are representative of 12:00 noon local time around the world.

The GEFF model, calculates the FWI by modelling fuel moisture response to atmospheric forces at different depths. Three  
fuel moisture levels are used, representing surface fuels, deeper organic material, and compact fuels, each responding at differ-  
ent rates to changes in weather. These moisture codes are then combined to estimate fire behaviour, such as the rate of spread  
and fire intensity, providing a comprehensive fire danger index.

690 The GEFF-ERA5 FWI reanalysis dataset is available from 1979 onwards, at a spatial resolution of 28 km.

When comparing datasets (modelled or observed) at different grid resolutions, the higher-resolution dataset is re-gridded to  
the lowest-resolution grid using a first-order conservative area-weighted re-gridding method.



## A2 Appendix and Tables

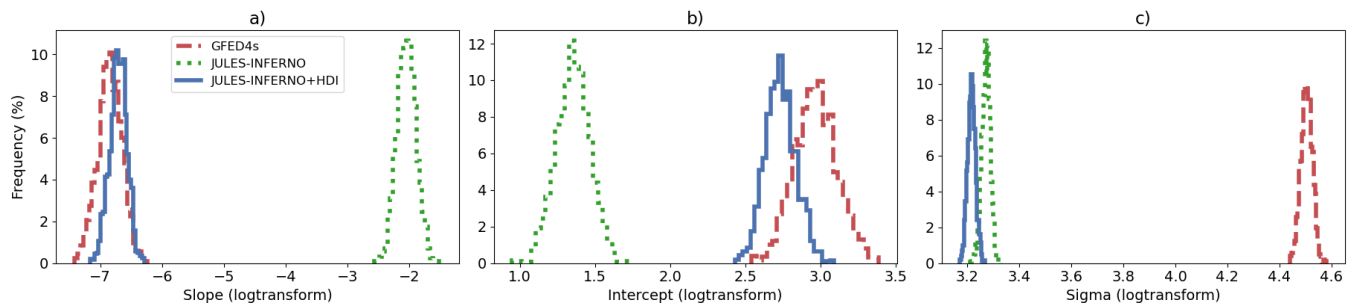


**Figure A2.** Histograms of posterior distributions for Bayesian linear regression fit parameters derived for GFED4s (dashed red line), JULES-INFERNO (dotted green line), and JULES-INFERNO+HDI (solid blue line). Panel a) shows the slope parameter, b) the intercept parameter, and c) depicts the sigma (error term representing random sampling noise) in log-transformed space.

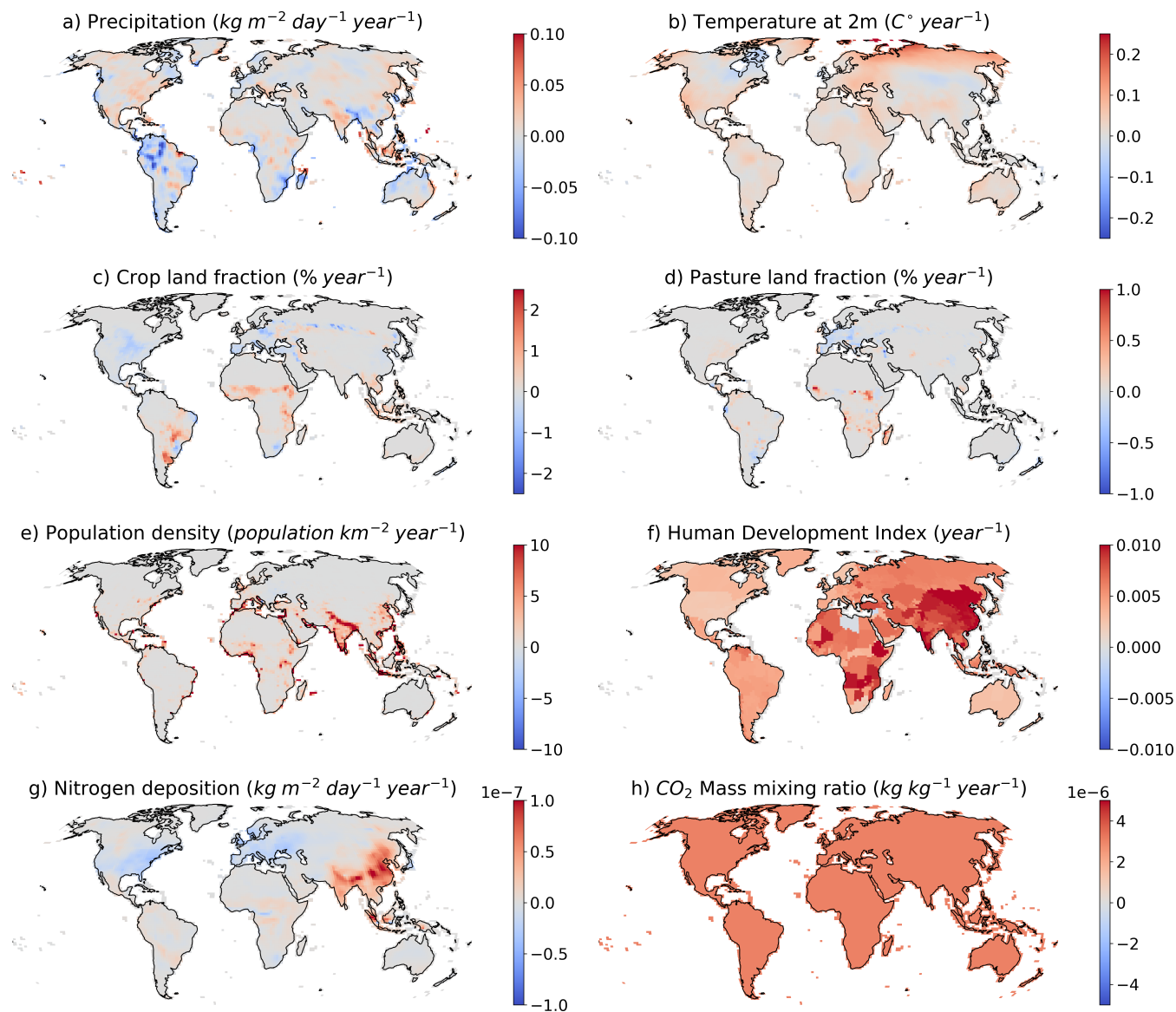


**Figure A3.** Trends calculated between the period 1997 - 2016 for JULES-ES external forcing variables a) Precipitation ( $kg\ m^{-2}\ day^{-1}\ year^{-1}$ ), b) Temperature at 2 m ( $C^{\circ}\ year^{-1}$ ), c) Crop land fraction ( $\%\ year^{-1}$ ), d) Pasture land fraction ( $\%\ year^{-1}$ ), e) Population density ( $population\ km^{-2}\ year^{-1}$ ), f) Human Development Index ( $year^{-1}$ ), g) Nitrogen deposition ( $kg\ m^{-2}\ day^{-1}\ year^{-1}$ ), and h) Carbon Dioxide mixing ratio ( $kg\ kg^{-1}\ year^{-1}$ ).



**Table A1.** Annual burnt area statistics for the different GFED4s fire regions (Giglio et al., 2013).

	GLOBAL	BONA	TENA	CEAM	NHSA	SHSA	EURO	MIDE	NHAF	SHAF	BOAS	CEAS	SEAS	EQAS	AUST
Mean BA (Mha)	476.43	2.47	2.33	1.68	4.94	25.85	0.86	0.90	152.24	155.85	7.65	19.22	12.85	0.70	39.88
Trend (Mha year <sup>-1</sup> )	-6.77	0.05	0.05	-0.04	-0.05	-0.44	-0.03	0.02	-2.20	-0.54	-0.03	-0.37	0.18	-0.02	-1.09
Mean BA (Mha)	442.08	4.09	19.53	6.08	1.97	75.09	3.09	4.78	136.30	85.29	10.21	14.88	13.89	0.11	31.43
Trend (Mha year <sup>-1</sup> )	-2.24	-0.02	0.09	0.00	0.02	-0.13	0.01	-0.04	-1.26	-0.14	0.05	0.10	0.08	0.00	0.02
Bias (Mha)	-34.35	1.62	17.21	4.40	-2.97	49.24	2.23	3.88	-15.94	-70.56	2.56	-4.34	1.03	-0.59	-8.46
Relative bias (%)	-7.21	65.27	739.79	262.03	-60.16	190.48	258.82	432.09	-10.47	-45.27	33.48	-22.58	8.05	-84.81	-21.20
RMSE	47.28	2.10	17.38	4.52	3.07	49.85	2.27	3.92	20.23	71.17	4.26	7.16	1.91	0.89	21.60
RMSE UE	32.50	1.35	2.43	1.00	0.77	7.78	0.45	0.55	12.45	9.31	3.40	5.69	1.60	0.66	19.87
Correlation (%)	75.25	0.22	81.58	54.76	58.26	47.88	15.35	-26.02	77.73	46.76	26.75	13.83	68.84	79.84	8.70
STD / STD <sub>GFED4s</sub>	0.39	0.25	4.47	0.84	0.69	0.77	0.68	1.00	0.75	0.44	0.23	0.22	0.54	0.10	0.18
RMSE / STD <sub>GFED4s</sub>	1.10	1.61	26.45	3.99	3.25	5.93	5.72	11.31	1.02	6.76	1.21	1.25	0.88	1.23	1.09
RMSE <sub>UE</sub> / STD <sub>GFED4s</sub>	0.75	1.03	3.70	0.89	0.82	0.93	1.12	1.59	0.63	0.88	0.96	0.99	0.74	0.92	1.00
Mean BA (Mha)	278.90	0.52	3.40	2.13	0.29	25.58	0.45	3.09	125.08	69.65	3.43	6.50	9.56	0.03	7.14
Trend (Mha year <sup>-1</sup> )	-7.58	-0.02	-0.07	-0.05	-0.01	-0.64	-0.01	-0.11	-2.71	-1.94	-0.09	-0.22	-0.19	0.00	-0.20
Bias (Mha)	-197.52	-1.95	1.07	0.45	-4.65	-0.27	-0.41	2.19	-27.16	-86.20	-4.22	-12.72	-3.30	-0.67	-32.74
Relative bias (%)	-41.46	-78.97	46.08	26.56	-94.14	-1.05	-48.14	244.36	-17.84	-55.31	-55.17	-66.19	-25.64	-95.88	-82.09
RMSE	198.99	2.37	1.34	1.03	4.73	7.87	0.53	2.35	29.19	87.11	5.44	13.80	4.23	0.97	38.14
RMSE <sub>UE</sub>	24.12	1.34	0.81	0.92	0.89	7.87	0.33	0.84	10.70	12.60	3.44	5.36	2.66	0.70	19.57
Correlation (%)	84.19	-14.08	39.06	61.37	64.10	37.74	73.22	-24.81	86.33	39.02	23.13	37.02	-6.63	85.02	21.62
STD / STD <sub>GFED4s</sub>	0.99	0.11	1.21	0.41	0.10	0.51	0.24	1.98	1.06	1.15	0.18	0.25	0.65	0.03	0.09
RMSE / STD <sub>GFED4s</sub>	4.61	1.81	2.04	0.91	5.01	0.94	1.34	6.78	1.48	8.27	1.54	2.41	1.95	1.35	1.92
RMSE <sub>UE</sub> / STD <sub>GFED4s</sub>	0.56	1.02	1.23	0.82	0.94	0.94	0.84	2.43	0.54	1.20	0.97	0.94	1.23	0.97	0.99



**Table A2.** JULES-INFERNO burnt area trends ( $Mha\ year^{-1}$ ) for the different GFED4s fire regions (Giglio et al., 2013) from the model sensitivity experiments. The standard error of the estimated trend, under the assumption of residual normality is shown in brackets. Values in bold represent trends that are significantly different from zero at the 99% confidence level.

	GFED4s	JULES-INFERNO								
		<i>control</i>	<i>1990 control</i>	<i>clim</i>	<i>tas</i>	<i>ppn</i>	<i>lu</i>	<i>Ndep</i>	<i>pop</i>	<i>CO2</i>
<b>GLOBAL</b>	<b>-6.77</b> (9.8e-01)	<b>-2.24</b> (5.1e-01)	-0.26 (5.3e-01)	-0.06 (5.5e-01)	0.42 (4.7e-01)	-0.92 (4.9e-01)	-1.01 (5.4e-01)	-0.27 (5.3e-01)	-1.45 (4.7e-01)	-0.32 (6.0e-01)
<b>BONA</b>	0.048 (5.2e-02)	-0.017 (1.3e-02)	0.002 (1.9e-03)	-0.023 (1.2e-02)	0.008 (1.5e-02)	-0.007 (7.7e-03)	0.003 (1.8e-03)	0.002 (1.8e-03)	0.005 (1.8e-03)	0.003 (1.8e-03)
<b>TENA</b>	0.05 (2.4e-02)	0.08 (1.2e-01)	0.01 (1.1e-02)	0.04 (1.1e-01)	0.08 (2.9e-02)	-0.05 (6.7e-02)	<b>0.05</b> (9.3e-03)	0.01 (1.2e-02)	-0.02 (1.1e-02)	0.05 (1.2e-02)
<b>CEAM</b>	-0.07 (4.3e-02)	0.000 (3.9e-02)	0.01 (9.1e-03)	0.03 (4.2e-02)	0.03 (1.4e-02)	0.02 (3.9e-02)	0.01 (8.6e-03)	0.01 (9.1e-03)	-0.01 (8.9e-03)	0.01 (9.2e-03)
<b>NHSA</b>	-0.05 (3.7e-02)	0.02 (2.6e-02)	0.001 (7.5e-04)	0.03 (2.6e-02)	0.01 (6.0e-03)	0.02 (1.8e-02)	0.002 (9.4e-04)	0.001 (7.5e-04)	-0.002 (7.9e-04)	-0.005 (1.5e-03)
<b>SHSA</b>	-0.41 (3.3e-01)	-0.12 (2.6e-01)	0.04 (8.3e-02)	0.14 (2.8e-01)	0.27 (7.3e-02)	-0.17 (2.2e-01)	-0.17 (8.6e-02)	0.04 (8.3e-02)	-0.005 (8.2e-02)	-0.01 (9.4e-02)
<b>EURO</b>	-0.03 (1.4e-02)	0.01 (1.1e-02)	0.001 (3.5e-03)	-0.001 (1.0e-02)	0.01 (3.9e-03)	-0.01 (7.4e-03)	<b>0.01</b> (2.0e-03)	0.0005 (3.4e-03)	-0.01 (3.5e-03)	0.003 (3.2e-03)
<b>MIDE</b>	0.02 (1.4e-02)	-0.04 (1.2e-02)	0.001 (7.8e-03)	-0.02 (1.3e-02)	0.01 (9.9e-03)	-0.04 (1.2e-02)	0.001 (7.8e-03)	-0.003 (9.4e-03)	<b>-0.04</b> (6.9e-03)	0.01 (7.6e-03)
<b>NHAF</b>	-2.24 (6.1e-01)	-1.35 (5.1e-01)	0.04 (3.1e-01)	0.15 (5.2e-01)	0.14 (3.2e-01)	-0.10 (5.3e-01)	-0.35 (3.3e-01)	0.04 (3.1e-01)	-0.55 (2.7e-01)	0.06 (3.2e-01)
<b>SHAF</b>	-0.53 (4.1e-01)	-0.15 (1.9e-01)	0.17 (1.4e-01)	0.27 (1.9e-01)	0.15 (1.4e-01)	0.15 (1.4e-01)	0.01 (1.4e-01)	0.17 (1.4e-01)	-0.18 (1.4e-01)	0.04 (1.6e-01)
<b>BOAS</b>	-0.07 (1.4e-01)	0.05 (3.1e-02)	0.01 (4.2e-03)	0.04 (2.9e-02)	0.06 (2.1e-02)	0.03 (1.5e-02)	0.02 (3.9e-03)	0.01 (4.0e-03)	-0.01 (3.9e-03)	0.01 (4.1e-03)
<b>CEAS</b>	-0.35 (2.2e-01)	0.10 (4.6e-02)	0.01 (7.3e-03)	0.08 (5.0e-02)	0.05 (2.4e-02)	0.03 (2.6e-02)	0.02 (8.0e-03)	0.01 (6.7e-03)	0.01 (7.5e-03)	0.03 (9.2e-03)
<b>SEAS</b>	0.17 (7.9e-02)	0.07 (4.4e-02)	0.02 (8.6e-03)	0.06 (4.3e-02)	0.03 (2.4e-02)	0.05 (3.3e-02)	0.0004 (7.6e-03)	0.02 (7.9e-03)	<b>0.04</b> (8.4e-03)	0.02 (9.0e-03)
<b>EQAS</b>	-0.04 (2.8e-02)	-0.0027 (3.0e-03)	0.0004 (2.2e-04)	-0.0020 (3.3e-03)	0.0003 (3.3e-04)	-0.0017 (2.5e-03)	-0.0001 (2.2e-04)	0.0004 (2.2e-04)	-0.0002 (2.0e-04)	0.0003 (2.2e-04)
<b>AUST</b>	-1.02 (7.8e-01)	0.01 (1.4e-01)	0.07 (5.6e-02)	-0.05 (1.5e-01)	0.12 (5.9e-02)	-0.12 (1.3e-01)	0.07 (5.6e-02)	0.06 (5.6e-02)	0.07 (5.6e-02)	0.11 (5.8e-02)



**Table A3.** JULES-INFERNO+HDI burnt area trends ( $Mha\ year^{-1}$ ) for the different GFED4s fire regions (Giglio et al., 2013) from the model sensitivity experiments. The standard error of the estimated trend, under the assumption of residual normality is shown in brackets. Values in bold represent trends that are significantly different from zero at the 99% confidence level.

	GFED4s	JULES-INFERNO+HDI									
		<i>control</i>	<i>1990 control</i>	<i>clim</i>	<i>tas</i>	<i>ppn</i>	<i>lu</i>	<i>Ndep</i>	<i>pop</i>	<i>CO2</i>	<i>HDI</i>
<b>GLOBAL</b>	<b>-6.77</b> (9.8e-01)	<b>0.15</b> (2.2e-02)	<b>-7.58</b> (4.2e-01)	0.24 (5.5e-01)	0.58 (2.1e-01)	-0.60 (5.5e-01)	<b>-0.97</b> (2.0e-02)	<b>0.16</b> (2.3e-02)	<b>-0.91</b> (1.9e-02)	0.02 (2.3e-02)	<b>-4.27</b> (9.8e-02)
<b>BONA</b>	0.048 (5.2e-02)	-0.0002 (8.2e-05)	<b>-0.023</b> (2.1e-03)	-0.006 (2.8e-03)	0.002 (2.8e-03)	-0.003 (1.9e-03)	-0.0002 (8.2e-05)	-0.0002 (8.3e-05)	-0.0003 (8.0e-05)	-0.0001 (8.1e-05)	<b>-0.021</b> (6.6e-04)
<b>TENA</b>	0.05 (2.4e-02)	0.00 (7.1e-04)	-0.07 (2.8e-02)	0.001 (3.6e-02)	0.02 (8.3e-03)	-0.02 (2.2e-02)	<b>0.01</b> (8.4e-04)	0.000 (8.3e-04)	<b>-0.01</b> (7.9e-04)	<b>0.004</b> (8.0e-04)	<b>-0.05</b> (1.7e-03)
<b>CEAM</b>	-0.07 (4.3e-02)	<b>-0.01</b> (1.5e-03)	-0.04 (1.6e-02)	0.02 (2.3e-02)	0.01 (3.8e-03)	0.01 (2.3e-02)	-0.01 (1.6e-03)	<b>-0.01</b> (1.5e-03)	<b>-0.02</b> (1.4e-03)	-0.01 (1.7e-03)	<b>-0.05</b> (1.5e-03)
<b>NHSA</b>	-0.05 (3.7e-02)	0.000 (1.2e-04)	-0.01 (3.7e-03)	0.01 (5.8e-03)	0.003 (1.5e-03)	0.003 (3.9e-03)	<b>-0.001</b> (1.0e-04)	-0.0005 (1.2e-04)	<b>-0.001</b> (1.3e-04)	<b>-0.004</b> (1.5e-04)	<b>-0.01</b> (4.7e-04)
<b>SHSA</b>	-0.41 (3.3e-01)	0.05 (2.1e-02)	<b>-0.62</b> (9.7e-02)	0.11 (1.4e-01)	<b>0.14</b> (3.1e-02)	-0.09 (1.1e-01)	-0.06 (2.4e-02)	0.05 (2.1e-02)	0.02 (2.1e-02)	-0.002 (2.3e-02)	<b>-0.34</b> (1.9e-02)
<b>EURO</b>	-0.03 (1.4e-02)	-0.0002 (1.2e-04)	<b>-0.01</b> (2.4e-03)	-0.0001 (3.1e-03)	<b>0.004</b> (9.2e-04)	-0.003 (2.1e-03)	<b>0.004</b> (1.3e-04)	-0.0002 (1.2e-04)	<b>-0.002</b> (1.5e-04)	<b>0.001</b> (1.3e-04)	<b>-0.01</b> (4.4e-04)
<b>MIDE</b>	0.02 (1.4e-02)	<b>0.02</b> (3.0e-03)	<b>-0.11</b> (8.9e-03)	-0.004 (1.5e-02)	<b>0.03</b> (5.7e-03)	-0.02 (1.5e-02)	<b>0.02</b> (2.6e-03)	<b>0.02</b> (4.4e-03)	<b>-0.03</b> (3.0e-03)	<b>0.04</b> (2.5e-03)	<b>-0.09</b> (4.8e-03)
<b>NHAF</b>	-2.24 (6.1e-01)	0.14 (7.1e-02)	<b>-2.78</b> (5.5e-01)	0.50 (6.3e-01)	0.33 (1.2e-01)	0.12 (6.0e-01)	<b>-0.57</b> (6.6e-02)	0.14 (7.2e-02)	<b>-0.31</b> (7.3e-02)	0.24 (7.6e-02)	<b>-0.73</b> (9.0e-02)
<b>SHAF</b>	-0.53 (4.1e-01)	0.29 (1.3e-01)	<b>-1.92</b> (2.1e-01)	0.28 (2.2e-01)	0.24 (1.5e-01)	0.05 (1.5e-01)	0.03 (1.3e-01)	0.30 (1.3e-01)	-0.09 (1.3e-01)	0.07 (1.3e-01)	<b>-1.48</b> (1.7e-01)
<b>BOAS</b>	-0.07 (1.4e-01)	0.001 (9.0e-04)	<b>-0.10</b> (1.3e-02)	0.02 (1.2e-02)	0.02 (6.2e-03)	0.02 (6.8e-03)	<b>0.005</b> (8.8e-04)	0.002 (9.3e-04)	-0.002 (8.7e-04)	0.003 (9.1e-04)	<b>-0.12</b> (5.0e-03)
<b>CEAS</b>	-0.35 (2.2e-01)	0.01 (5.0e-03)	<b>-0.23</b> (2.3e-02)	0.04 (3.1e-02)	0.04 (1.2e-02)	0.02 (1.7e-02)	<b>0.02</b> (4.5e-03)	0.02 (4.4e-03)	0.01 (5.0e-03)	<b>0.03</b> (4.9e-03)	<b>-0.23</b> (8.1e-03)
<b>SEAS</b>	0.17 (7.9e-02)	0.02 (7.7e-03)	<b>-0.19</b> (3.5e-02)	0.08 (4.5e-02)	0.04 (2.5e-02)	0.06 (3.7e-02)	0.004 (7.4e-03)	0.02 (7.0e-03)	<b>0.04</b> (7.6e-03)	0.02 (7.6e-03)	<b>-0.19</b> (7.7e-03)
<b>EQAS</b>	-0.04 (2.8e-02)	0.0003 (1.1e-04)	-0.0014 (8.3e-04)	-0.0005 (1.3e-03)	0.0003 (1.3e-04)	-0.0005 (9.9e-04)	-0.0001 (1.1e-04)	0.0003 (1.1e-04)	0.0001 (9.5e-05)	0.0002 (1.1e-04)	<b>-0.001</b> (1.0e-04)
<b>AUST</b>	-1.02 (7.8e-01)	0.03 (1.9e-02)	-0.19 (5.3e-02)	0.01 (7.2e-02)	0.06 (2.5e-02)	-0.01 (6.5e-02)	0.03 (1.9e-02)	0.03 (1.9e-02)	0.03 (1.9e-02)	0.04 (1.9e-02)	<b>-0.17</b> (1.6e-02)



*Code and data availability.* Both the model code and the files for running it are available from the Met Office Science Repository Service:  
695 <https://code.metoffice.gov.uk/> (last access: 26 July 2023). Registration is required, and code is freely available subject to completion of a software license.

Details of the simulations performed: JULES simulations are compiled and run in suites developed using the Rose suite engine (MetOffice, 2022) and scheduled using the cylc workflow engine (Oliver et al., 2019). Both Rose and cylc are available under v3 of the GNU General Public License (GPL). In this framework, the suite contains the information required to extract and build the code as well as configure and  
700 run the simulations. Each suite is labelled with a unique identifier and is held in the same revision-controlled repository service in which we hold and develop the model code. This means that these suites are available to any licensed of JULES under the following suite IDs:

- JULES-INFERNO: u-by849
- JULES-INFERNO+HDI: u-by851

For JULES-INFERNO sensitivity experiments:

- 705 – 1990 control: u-co594
- clim: u-cs067
- tas: u-cs068
- ppn: u-cs069
- lu: u-cr440
- 710 – Ndep: u-cr441
- pop: u-cr442
- CO<sub>2</sub>: u-cr443

For JULES-INFERNO+HDI sensitivity experiments:

- 1990 control: u-ct759
- 715 – clim: u-cs070
- tas: u-cs071
- ppn: u-cs072
- lu: u-cr447
- Ndep: u-cr448
- 720 – pop: u-cr449
- CO<sub>2</sub>: u-cr450
- HDI: u-cn957

*Author contributions.* JCMT led the writing of the paper and model development. All co-authors contributed to the simulation design, writing sections, performing evaluation and reviewing drafts of the paper.



725 *Competing interests.* At least one of the (co-)authors is a member of the editorial board of Earth System Dynamics.

*Acknowledgements.* We would especially like to thank those who have contributed to the development of INFERNO, with a special thanks to Stéphane Mangeon for taking the first steps to develop INFERNO and the observational community, who have developed numerous datasets used in this paper to help evaluate the model.

This research and JCMT, CB, GAF, FMOC, RAB were supported by the Met Office Hadley Centre Climate Programme funded by DSIT. 730 JCMT, GAF, and FMOC were also supported by the Horizon 2020 Framework Programme (CRESCENDO, grant no. 779366) and the Earth System Models for the Future (ESM2025, grant no. 101003536). CB was funded by the Met Office Climate Science for Service Partnership (CSSP) Brazil project which is supported by the Department for Science, Innovation & Technology (DSIT). DIK was supported by the Natural Environment Research Council as part of the LTSM2 TerraFIRMA project. AV was funded via the Leverhulme Centre for Wildfires, Environment and Society through the Leverhulme Trust, grant no. RC-2018-023.



## 735 References

- Abatzoglou, J. T. and Williams, A. P.: Impact of anthropogenic climate change on wildfire across western US forests, *Proceedings of the National Academy of Sciences*, 113, 11 770–11 775, 2016.
- Abatzoglou, J. T., Williams, A. P., Boschetti, L., Zubkova, M., and Kolden, C. A.: Global patterns of interannual climate–fire relationships, *Global change biology*, 24, 5164–5175, 2018.
- 740 Andela, N. and Van Der Werf, G. R.: Recent trends in African fires driven by cropland expansion and El Nino to La Nina transition, *Nature Climate Change*, 4, 791–795, 2014.
- Andela, N., Morton, D. C., Giglio, L., Chen, Y., van der Werf, G. R., Kasibhatla, P. S., DeFries, R. S., Collatz, G., Hantson, S., Kloster, S., et al.: A human-driven decline in global burned area, *Science*, 356, 1356–1362, 2017.
- Andela, N., Morton, D. C., Giglio, L., Paugam, R., Chen, Y., Hantson, S., Van Der Werf, G. R., and Randerson, J. T.: The Global Fire Atlas  
745 of individual fire size, duration, speed and direction, *Earth System Science Data*, 11, 529–552, 2019.
- Aragão, L. E., Anderson, L. O., Fonseca, M. G., Rosan, T. M., Vedovato, L. B., Wagner, F. H., Silva, C. V., Silva Junior, C. H., Arai, E., Aguiar, A. P., et al.: 21st Century drought-related fires counteract the decline of Amazon deforestation carbon emissions, *Nature communications*, 9, 536, 2018.
- Archibald, S., Nickless, A., Govender, N., Scholes, R. J., and Lehsten, V.: Climate and the inter-annual variability of fire in southern Africa:  
750 a meta-analysis using long-term field data and satellite-derived burnt area data, *Global Ecology and Biogeography*, 19, 794–809, 2010.
- Best, M. J., Pryor, M., Clark, D. B., Rooney, G. G., Essery, R. L. H., Ménard, C. B., Edwards, J. M., Hendry, M. A., Porson, A., Gedney, N., Mercado, L. M., Sitch, S., Blyth, E., Boucher, O., Cox, P. M., Grimmond, C. S. B., and Harding, R. J.: The Joint UK Land Environment Simulator (JULES), model description – Part 1: Energy and water fluxes, *Geoscientific Model Development*, 4, 677–699, <https://doi.org/10.5194/gmd-4-677-2011>, 2011.
- 755 Bhanojirao, V.: Human development report 1990: review and assessment, *World Development*, 19, 1451–1460, 1991.
- Blackford, K. R., Kasoar, M., Burton, C., Burke, E., Prentice, I. C., and Voulgarakis, A.: INFERNO-peat v1. 0.0: a representation of northern high-latitude peat fires in the JULES-INFERNO global fire model, *Geoscientific Model Development*, 17, 3063–3079, 2024.
- Bowman, D. M., Kolden, C. A., Abatzoglou, J. T., Johnston, F. H., van der Werf, G. R., and Flannigan, M.: Vegetation fires in the Anthropocene, *Nature Reviews Earth & Environment*, 1, 500–515, 2020.
- 760 Burton, C., Betts, R., Cardoso, M., Feldpausch, T. R., Harper, A., Jones, C. D., Kelley, D. I., Robertson, E., and Wiltshire, A.: Representation of fire, land-use change and vegetation dynamics in the Joint UK Land Environment Simulator vn4.9 (JULES), *Geoscientific Model Development*, 12, 179–193, <https://doi.org/10.5194/gmd-12-179-2019>, 2019.
- Burton, C., Betts, R. A., Jones, C. D., Feldpausch, T. R., Cardoso, M., and Anderson, L. O.: El Niño Driven Changes in Global Fire 2015/16, *Frontiers in Earth Science*, 8, 199, <https://doi.org/10.3389/feart.2020.00199>, 2020.
- 765 Carreiras, M., Ferreira, A. J. D., Valente, S., Fleskens, L., Gonzales-Pelayo, Ó., Rubio, J. L., Stoof, C. R., Coelho, C. O. A., Ferreira, C. S. S., and Ritsema, C. J.: Comparative analysis of policies to deal with wildfire risk, *Land Degradation & Development*, 25, 92–103, 2014.
- Cecil, D.: LIS/OTD 0.5 Degree High Resolution Monthly Climatology (HRMC), <https://doi.org/10.3389/feart.2020.00199>, 2006.
- Chergui, B., Fahd, S., Santos, X., and Pausas, J. G.: Socioeconomic factors drive fire-regime variability in the Mediterranean Basin, *Ecosystems*, 21, 619–628, 2018.
- 770 Chuvieco, E., Pettinari, M. L., Koutsias, N., Forkel, M., Hantson, S., and Turco, M.: Human and climate drivers of global biomass burning variability, *Science of the Total Environment*, 779, 146 361, 2021.



- Clark, D. B., Mercado, L. M., Sitch, S., Jones, C. D., Gedney, N., Best, M. J., Pryor, M., Rooney, G. G., Essery, R. L. H., Blyth, E., Boucher, O., Harding, R. J., Huntingford, C., and Cox, P. M.: The Joint UK Land Environment Simulator (JULES), model description – Part 2: Carbon fluxes and vegetation dynamics, *Geoscientific Model Development*, 4, 701–722, <https://doi.org/10.5194/gmd-4-701-2011>, 2011.
- 775 Cox, P.: Description of the "TRIFFID" Dynamic Global Vegetation Mode, 2001.
- Cox, P., Betts, R., Jones, C., Spall, S., and Totterdell, I.: Acceleration of global warming due to carbon-cycle feedbacks in a coupled climate model, *Nature*, 408, 184–187, 2000.
- Curt, T. and Frejaville, T.: Wildfire policy in Mediterranean France: how far is it efficient and sustainable?, *Risk analysis*, 38, 472–488, 2018.
- Duane, A., Aquilué, N., Canelles, Q., Morán-Ordoñez, A., De Cáceres, M., and Brotons, L.: Adapting prescribed burns to future climate change in Mediterranean landscapes, *Science of the Total Environment*, 677, 68–83, 2019.
- 780 Eyring, V., Bony, S., Meehl, G. A., Senior, C. A., Stevens, B., Stouffer, R. J., and Taylor, K. E.: Overview of the Coupled Model Intercomparison Project Phase 6 (CMIP6) experimental design and organization, *Geoscientific Model Development*, 9, 1937–1958, 2016.
- Ford, A. E., Harrison, S. P., Kountouris, Y., Millington, J. D., Mistry, J., Perkins, O., Rabin, S. S., Rein, G., Schreckenber, K., Smith, C., et al.: Modelling human-fire interactions: combining alternative perspectives and approaches, *Frontiers in Environmental Science*, p. 418, 785 2021.
- Giglio, L., Randerson, J. T., and Van Der Werf, G. R.: Analysis of daily, monthly, and annual burned area using the fourth-generation global fire emissions database (GFED4), *Journal of Geophysical Research: Biogeosciences*, 118, 317–328, 2013.
- Gillson, L., Whitlock, C., and Humphrey, G.: Resilience and fire management in the Anthropocene, *Ecology and Society*, 24, 2019.
- Goldewijk, K. K., Dekker, S. C., and van Zanden, J. L.: Per-capita estimations of long-term historical land use and the consequences for global change research, *Journal of Land Use Science*, 12, 313–337, <https://doi.org/10.1080/1747423X.2017.1354938>, 2017.
- 790 Goss, M., Swain, D. L., Abatzoglou, J. T., Sarhadi, A., Kolden, C. A., Williams, A. P., and Diffenbaugh, N. S.: Climate change is increasing the likelihood of extreme autumn wildfire conditions across California, *Environmental Research Letters*, 15, 094016, 2020.
- Haas, O., Prentice, I. C., and Harrison, S. P.: Global environmental controls on wildfire burnt area, size, and intensity, *Environmental Research Letters*, 17, 065004, 2022.
- 795 Haas, O., Prentice, I., and Harrison, S.: Global wildfires on a changing planet - in review, 2024.
- Harris, I., Jones, P. D., Osborn, T. J., and Lister, D. H.: Updated high-resolution grids of monthly climatic observations—the CRU TS3. 10 Dataset, *International journal of climatology*, 34, 623–642, 2014.
- Hickel, J.: The sustainable development index: Measuring the ecological efficiency of human development in the anthropocene, *Ecological economics*, 167, 106331, 2020.
- 800 Jacobson, M., Smith, H., Huber-Stearns, H. R., Davis, E. J., Cheng, A. S., and Deak, A.: Comparing social constructions of wildfire risk across media, government, and participatory discourse in a Colorado fireshed, *Journal of Risk Research*, 25, 697–714, 2022.
- Jones, M. W., Abatzoglou, J. T., Veraverbeke, S., Andela, N., Lasslop, G., Forkel, M., Smith, A. J., Burton, C., Betts, R. A., van der Werf, G. R., et al.: Global and regional trends and drivers of fire under climate change, *Reviews of Geophysics*, p. e2020RG000726, 2022.
- Jones, M. W., Kelley, D. I., Burton, C. A., Di Giuseppe, F., Barbosa, M. L. F., Brambleby, E., Hartley, A. J., Lombardi, A., Mataveli, G., 805 McNorton, J. R., et al.: State of wildfires 2023–2024, *Earth System Science Data*, 16, 3601–3685, 2024.
- Kasischke, E. S. and Turetsky, M. R.: Recent changes in the fire regime across the North American boreal region—Spatial and temporal patterns of burning across Canada and Alaska, *Geophysical research letters*, 33, 2006.
- Kelley, D. I., Bistinas, I., Whitley, R., Burton, C., Marthews, T. R., and Dong, N.: How contemporary bioclimatic and human controls change global fire regimes, *Nature Climate Change*, 9, 690–696, 2019.



- 810 Kirillina, K., Shvetsov, E. G., Protopopova, V. V., Thiesmeyer, L., and Yan, W.: Consideration of anthropogenic factors in boreal forest fire regime changes during rapid socio-economic development: case study of forestry districts with increasing burnt area in the Sakha Republic, Russia, *Environmental Research Letters*, 15, 035 009, 2020.
- Klaunberg, K., Wübbeler, G., Mickan, B., Harris, P., and Elster, C.: A tutorial on Bayesian normal linear regression, *Metrologia*, 52, 878, 2015.
- 815 Klein Goldewijk, K., Beusen, A., Doelman, J., and Stehfest, E.: Anthropogenic land use estimates for the Holocene – HYDE 3.2, *Earth System Science Data*, 9, 927–953, <https://doi.org/10.5194/essd-9-927-2017>, 2017.
- Kummu, M., Taka, M., and Guillaume, J. H.: Gridded global datasets for gross domestic product and Human Development Index over 1990–2015, *Scientific data*, 5, 180 004, 2018.
- Li, F., Levis, S., and Ward, D.: Quantifying the role of fire in the Earth system—Part I: Improved global fire modeling in the Community Earth System Model (CESM1), *Biogeosciences*, 10, 2293–2314, 2013.
- 820 Li, F., Song, X., Harrison, S. P., Marlon, J. R., Lin, Z., Leung, L. R., Schwinger, J., Marécal, V., Wang, S., Ward, D. S., et al.: Evaluation of global fire simulations in CMIP6 Earth system models, *Geoscientific Model Development Discussions*, 2024, 1–37, 2024.
- Mangeon, S., Voulgarakis, A., Gilham, R., Harper, A., Sitch, S., and Folberth, G.: INFERNO: a fire and emissions scheme for the UK Met Office’s Unified Model, *Geoscientific Model Development*, 9, 2685–2700, 2016.
- 825 Mathison, C., Burke, E., Hartley, A. J., Kelley, D. I., Burton, C., Robertson, E., Gedney, N., Williams, K., Wiltshire, A., Ellis, R. J., et al.: Description and Evaluation of the JULES-ES setup for ISIMIP2b, *EGUsphere*, 2022, 1–24, 2022.
- MetOffice: Rose suite engine, <https://metomi.github.io/rose/doc/html/index.html>, 2022.
- Miranda-Lescano, R., Muinel-Gallo, L., and Roca-Sagalés, O.: Human development and decentralization: The importance of public health expenditure, *Annals of Public and Cooperative Economics*, 94, 191–219, 2023.
- 830 Mourão, P. R. and Martinho, V. D.: The choices of the fire—Debating socioeconomic determinants of the fires observed at Portuguese municipalities, *Forest Policy and Economics*, 43, 29–40, 2014.
- Nepstad, D., McGrath, D., Stickler, C., Alencar, A., Azevedo, A., Swette, B., Bezerra, T., DiGiano, M., Shimada, J., Seroa da Motta, R., et al.: Slowing Amazon deforestation through public policy and interventions in beef and soy supply chains, *science*, 344, 1118–1123, 2014.
- 835 Nikolakis, W. and Roberts, E.: Wildfire governance in a changing world: Insights for policy learning and policy transfer, *Risk, Hazards & Crisis in Public Policy*, 13, 144–164, 2022.
- Oliver, H., Shin, M., Matthews, D., Sanders, O., Bartholomew, S., Clark, A., Fitzpatrick, B., van Haren, R., Hut, R., and Drost, N.: Workflow automation for cycling systems, *Computing in Science & Engineering*, 21, 7–21, 2019.
- Pandey, P., Huidobro, G., Lopes, L. F., Ganteaume, A., Ascoli, D., Colaco, C., Xanthopoulos, G., Giannaros, T. M., Gazzard, R., Boustras, G., et al.: A global outlook on increasing wildfire risk: Current policy situation and future pathways, *Trees, Forests and People*, 14, 100 431, 2023.
- 840 Paveglio, T. B., Carroll, M. S., Stasiewicz, A. M., Williams, D. R., and Becker, D. R.: Incorporating social diversity into wildfire management: Proposing “pathways” for fire adaptation, *Forest Science*, 64, 515–532, 2018.
- Pechony, O. and Shindell, D.: Fire parameterization on a global scale, *Journal of Geophysical Research: Atmospheres*, 114, 2009.
- 845 Perkins, O., Kasoar, M., Voulgarakis, A., Smith, C., Mistry, J., and Millington, J. D.: A global behavioural model of human fire use and management: WHAM! v1. 0, *Geoscientific Model Development*, 17, 3993–4016, 2024.



- Pivello, V. R., Vieira, I., Christianini, A. V., Ribeiro, D. B., da Silva Menezes, L., Berlinck, C. N., Melo, F. P., Marengo, J. A., Tornquist, C. G., Tomas, W. M., et al.: Understanding Brazil's catastrophic fires: Causes, consequences and policy needed to prevent future tragedies, *Perspectives in Ecology and Conservation*, 19, 233–255, 2021.
- 850 Prestemon, J. P., Butry, D. T., Abt, K. L., and Sutphen, R.: Net benefits of wildfire prevention education efforts, *Forest Science*, 56, 181–192, 2010.
- Rabin, S. S., Melton, J. R., Lasslop, G., Bachelet, D., Forrest, M., Hantson, S., Kaplan, J. O., Li, F., Mangeon, S., Ward, D. S., et al.: The Fire Modeling Intercomparison Project (FireMIP), phase 1: experimental and analytical protocols with detailed model descriptions, *Geoscientific Model Development*, 10, 1175–1197, 2017.
- 855 Randerson, J., Chen, Y., Van Der Werf, G., Rogers, B., and Morton, D.: Global burned area and biomass burning emissions from small fires, *Journal of Geophysical Research: Biogeosciences*, 117, 2012.
- Rideout, D. B., Wei, Y., Kirsch, A., and Kernohan, N.: STARFire: Strategic budgeting and planning for wildland fire management, *Park Science*, 32, 34–41, 2017.
- Riley, K. L., Williams, A. P., Urbanski, S. P., Calkin, D. E., Short, K. C., and O'Connor, C. D.: Will landscape fire increase in the future? A systems approach to climate, fire, fuel, and human drivers, *Current Pollution Reports*, 5, 9–24, 2019.
- 860 Rizzo, L. V. and Rizzo, M. C. F.: Wildfire smoke and health impacts: a narrative review, *Jornal de Pediatria*, 2024.
- Roy, A., Dutta, T., Li, Y., and Dong, X.: Human development at the cost of the environment?—an application of planetary pressures—adjusted human development index in the lens of planetary boundaries, *Environmental Science and Pollution Research*, 30, 32 383–32 405, 2023.
- Sellar, A. A., Jones, C. G., Mulcahy, J. P., Tang, Y., Yool, A., Wiltshire, A., O'Connor, F. M., Stringer, M., Hill, R., Palmieri, J., Woodward, S., de Mora, L., Kuhlbrodt, T., Rumbold, S. T., Kelley, D. I., Ellis, R., Johnson, C. E., Walton, J., Abraham, N. L., Andrews, M. B., Andrews, T., Archibald, A. T., Berthou, S., Burke, E., Blockley, E., Carslaw, K., Dalvi, M., Edwards, J., Folberth, G. A., Gedney, N., Griffiths, P. T., Harper, A. B., Hendry, M. A., Hewitt, A. J., Johnson, B., Jones, A., Jones, C. D., Keeble, J., Liddicoat, S., Morgenstern, O., Parker, R. J., Predoi, V., Robertson, E., Siahhaan, A., Smith, R. S., Swaminathan, R., Woodhouse, M. T., Zeng, G., and Zerroukat, M.: UKESM1: Description and Evaluation of the U.K. Earth System Model, *Journal of Advances in Modeling Earth Systems*, 11, 4513–4558, 865 <https://doi.org/https://doi.org/10.1029/2019MS001739>, 2019a.
- Sellar, A. A., Jones, C. G., Mulcahy, J. P., Tang, Y., Yool, A., Wiltshire, A., O'connor, F. M., Stringer, M., Hill, R., Palmieri, J., et al.: UKESM1: Description and evaluation of the UK Earth System Model, *Journal of Advances in Modeling Earth Systems*, 11, 4513–4558, 2019b.
- Silva Junior, C. H., Pessôa, A. C., Carvalho, N. S., Reis, J. B., Anderson, L. O., and Aragão, L. E.: The Brazilian Amazon deforestation rate 875 in 2020 is the greatest of the decade, *Nature Ecology & Evolution*, 5, 144–145, 2021.
- Stocks, B., Mason, J., Todd, J., Bosch, E., Wotton, B., Amiro, B., Flannigan, M., Hirsch, K., Logan, K., Martell, D., et al.: Large forest fires in Canada, 1959–1997, *Journal of Geophysical Research: Atmospheres*, 107, FFR–5, 2002.
- Sullivan, A., Kurvits, T., and E., B.: Spreading like Wildfire – The Rising Threat of Extraordinary Landscape Fires., United Nations Environment Programme (UNEP), 2022.
- 880 Teckentrup, L., Harrison, S. P., Hantson, S., Heil, A., Melton, J. R., Forrest, M., Li, F., Yue, C., Arneith, A., Hickler, T., et al.: Response of simulated burned area to historical changes in environmental and anthropogenic factors: a comparison of seven fire models, *Biogeosciences*, 16, 3883–3910, 2019.
- Teixeira, J. C., Folberth, G. A., O'Connor, F. M., Unger, N., and Voulgarakis, A.: Coupling interactive fire with atmospheric composition and climate in the UK Earth System Model, *Geoscientific Model Development*, 14, 6515–6539, 2021.



- 885 Türe, C.: A methodology to analyse the relations of ecological footprint corresponding with human development index: eco-sustainable human development index, *International Journal of Sustainable Development & World Ecology*, 20, 9–19, 2013.
- Urbieto, I. R., Franquesa, M., Viedma, O., and Moreno, J. M.: Fire activity and burned forest lands decreased during the last three decades in Spain, *Annals of Forest Science*, 76, 1–13, 2019.
- Veraverbeke, S., Rogers, B. M., Goulden, M. L., Jandt, R. R., Miller, C. E., Wiggins, E. B., and Randerson, J. T.: Lightning as a major driver of recent large fire years in North American boreal forests, *Nature Climate Change*, 7, 529–534, 2017.
- 890 Viovy, N.: CRUNCEP version 7-atmospheric forcing data for the community land model, Research Data Archive at the National Center for Atmospheric Research, Computational and Information Systems Laboratory, 10, 2018.
- Vitolo, C., Di Giuseppe, F., Barnard, C., Coughlan, R., San-Miguel-Ayanz, J., Libertá, G., and Krzeminski, B.: ERA5-based global meteorological wildfire danger maps, *Scientific data*, 7, 216, 2020.
- 895 Williams, A. P., Abatzoglou, J. T., Gershunov, A., Guzman-Morales, J., Bishop, D. A., Balch, J. K., and Lettenmaier, D. P.: Observed impacts of anthropogenic climate change on wildfire in California, *Earth's Future*, 7, 892–910, 2019.
- Williams, K., Copley, D., Blockley, E., Bodas-Salcedo, A., Calvert, D., Comer, R., Davis, P., Graham, T., Hewitt, H., Hill, R., et al.: The Met Office global coupled model 3.0 and 3.1 (GC3. 0 and GC3. 1) configurations, *Journal of Advances in Modeling Earth Systems*, 10, 357–380, 2018.
- 900 Zou, Y., Wang, Y., Ke, Z., Tian, H., Yang, J., and Liu, Y.: Development of a REgion-specific ecosystem feedback fire (RESFire) model in the Community Earth System Model, *Journal of Advances in Modeling Earth Systems*, 11, 417–445, 2019.
- Zubkova, M., Boschetti, L., Abatzoglou, J. T., and Giglio, L.: Changes in fire activity in Africa from 2002 to 2016 and their potential drivers, *Geophysical research letters*, 46, 7643–7653, 2019.